Chapter 4

The L84 Model

4.1 From Lorenz-63 to Lorenz-84

Results from the experiments conducted with the L63 model offered insight into the potential value of IC ensemble based experiments to explore uncertainty in the behaviour of the climate system. It was argued that sufficiently accounting for IC uncertainty not only benefits short- to medium-term weather forecasting but might also aid long time scale climate change prediction. The results highlighted the possible impacts of forcing variations on the climate system and the associated climate distributions. Going beyond the L63 model experiments, the primary aim of the work presented in this chapter is to gain additional insight by analysing the behaviour of a nonlinear chaotic system which can be more directly related to the climate system.

The Lorenz-84 (hereafter L84) model was described by Edward Lorenz as "the simplest possible model capable of representing an unmodified or modified Hadley circulation" (Lorenz (1984)). The model has subsequently been used by many researchers to make inferences about the behaviour of the climate system (e.g. Van Veen et al. (2001), Broer et al. (2002), Freire et al. (2008), Broer and Vitolo (2008)). Here, the model is examined to further understand how sensitive the climate of a nonlinear dynamic system is to changes in the system's forcing parameters. The experiments outlined in this chapter have been designed to determine the extent to which the predictability of the model's climate distributions is a function of the model's initial state. The ultimate goal of performing experiments with the L84 model is to develop hypotheses to inform the design of experiments to be conducted on more complex climate models.

In the L63 model, for $\rho > \rho_H$, the model displays *transitive* behaviour[1]. One of the primary reasons for performing additional experiments with the L84 model is that, at certain parameter values, the model contains coexisting attractors which display *intransitive* behaviour[1] (Lorenz (1984), Freire et al. (2008)). The conceptual challenge of understanding what constitutes climate and climate change in a system which displays intransitivity is examined using the L84 model.

[1]Definitions provided in the glossary.

It is demonstrated that the definition of climate in a system with coexisting attractors is not trivial and therefore interpreting climate under climate change is as much a communication problem as it is a simulation problem.

Adopting the methodology used for analysing the L63 model, this chapter first illustrates the climate of the L84 model for fixed parameter values. The plots focus on the distributions in the X variable, though the results for the Y and Z variables are qualitatively consistent and appear in Appendix B where relevant. In section 4.2, the attractor of the L84 model is illustrated for both chaotic and non-chaotic regions of parameter space. Section 4.3 displays the climate distributions resulting from single model trajectories and IC ensembles. This section begins with a visual analysis of the model climates followed by a quantitative analysis exploring the ergodic hypothesis. A seasonal cycle in one of the key parameters, F (the equator-to-pole temperature difference) is then introduced in section 4.4 and the impacts on the model climate distributions are presented. Maintaining the seasonal variations in F, in section 4.5 trends are imposed on F to further the analogy to modelling climate change. In section 4.6, the implications of the model results are discussed in relation to the design of experiments on more complex climate models.

4.2 The L84 System

4.2.1 The L84 model

Consistent with the approach used in chapter three, in the analysis of the L84 system the PMS is adopted so that the L84 model is equivalent to the L84 system. The model, used in this chapter to draw analogies to the climate system, is a simplified representation of the quasi-geostrophic equations and is defined by the three ODEs:

$$\frac{dX}{dt} = -Y^2 - Z^2 - aX + aF \tag{4.1}$$

$$\frac{dY}{dt} = XY - bXZ - Y + G \tag{4.2}$$

$$\frac{dZ}{dt} = bXY + XZ - Z \tag{4.3}$$

where X denotes the strength of the large-scale westerly wind current, assumed to be in equilibrium with the poleward temperature gradient, and Y and Z are the strength of cosine and sine phases of a chain of superposed waves transporting heat polewards. The term b represents the displacement of the waves due to interaction with the westerly wind and the term a is a coefficient which, if less than 1, allows the westerly wind current to damp less rapidly than the waves. F and G are thermal forcings: F represents the cross-latitude heating contrast (equator-to-pole temperature difference) and G accounts for the heating contrast between oceans and continents. A time unit in the L84 model is considered in relation to the damping time of the waves, which Lorenz equated to 5 days in the atmosphere (Lorenz (1984)). The time step used in Lorenz' original paper is $\tau = \frac{1}{30}$, equivalent to 4 hours, but for the following experiments a smaller time step, $\tau = 0.01$ (equivalent to 1.2 hours), is chosen with a common fourth order Runge-Kutta (RK) integration scheme as applied in chapter 3. The sensitivity of the model climate to the time step is investigated in section 4.3.2.

Lorenz (1990) imposed a seasonal variation in the parameter F to demonstrate that chaos and/or irregular dynamic behaviour can lead to interannual variability, manifest in the "random" onset of alternative periodic summer circulations. Adapting the seasonal variations introduced by Lorenz (1990), the impact of IC uncertainty is investigated in relation to the ergodicity of the L84 model and the memory of the system's climate distributions in the PMS. The following analysis examines the behaviour of the L84 model in what Lorenz termed "winter" and "summer" parameter conditions. Initially the idealised cases of permanent winter and permanent summer are investigated. In section 4.4, a seasonal cycle in F is introduced and the impact on the model's climate distributions is explored.

4.2.2 L84 in winter

In L84 winter, $F = 8$ and the other parameters are given their conventional values: $a = \frac{1}{4}$, $b = 4$ and $G = 1$. Figure 4.1 shows the three-dimensional evolution of a single trajectory orbiting the L84 attractor for permanent winter conditions over a period of 1 year. Figure 4.2 shows the same model run illustrated in two dimensions for the X-Y, X-Z and Y-Z planes. At first the trajectory orbits the primary 'lobe' (or regime) of the attractor, where $X > 0$, and subsequently spirals out away from the origin; the spiralling is most evident in the Y-Z plane shown in figure 4.2(c). The majority of the time the flow is westerly ($X > 0$) but occasionally the trajectory moves across to the secondary 'lobe', where $X < 0$. Physically, the transition to negative values of X represents a shift from westerly to easterly circulation. In the winter configuration the system is chaotic so small differences in the initial model states ultimately lead to large differences in the timing of transitions for individual model trajectories.

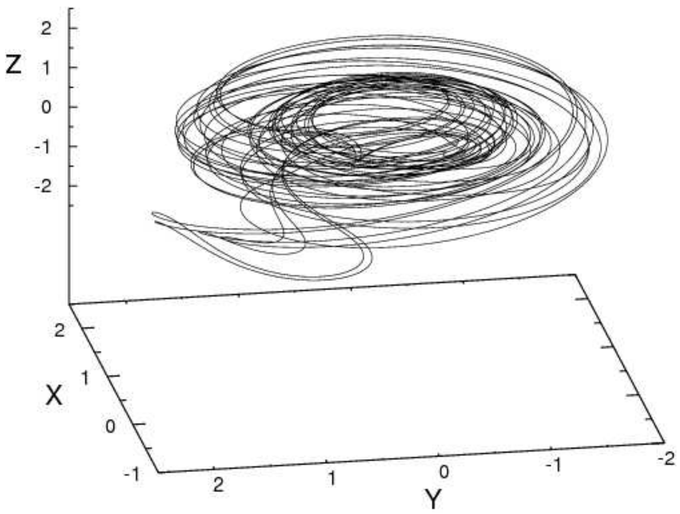

Figure 4.1: The L84 model attractor when $F = 8$ illustrated using a single trajectory over a simulation period of 1 year with ICs: $(X, Y, Z) = (1.0, 1.0, 1.0)$.

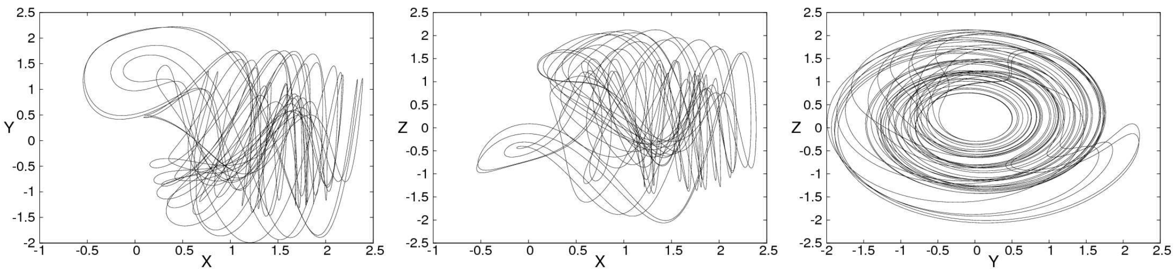

(a) X-Y Plane

(b) X-Z Plane

(c) Y-Z Plane

Figure 4.2: The L84 model attractor in the X-Y, X-Z and Y-Z planes when $F = 8$, illustrated using a single trajectory over a simulation period of 1 year with ICs: $(X, Y, Z) = (1.0, 1.0, 1.0)$.

4.2.3 L84 in summer

In the atmosphere, the meridional temperature difference between the pole and the equator is decreased during the summer months as the pole heats up, due to increased solar insolation, while the heating of the equator remains largely constant throughout the year. Lorenz (1990) encapsulates this change in the L84 model by suggesting a value of $F = 6$ for the summer configuration while keeping the other parameters constant. It is worth noting that one could decrease or even change the sign of G during the summer months where the land-sea temperature contrast is typically reversed. However, Lorenz (1990) keeps G constant and focuses his analysis on altered values of F only. In order to be consistent with the Lorenz (1990) study, the value of G is left unchanged in the following analysis.

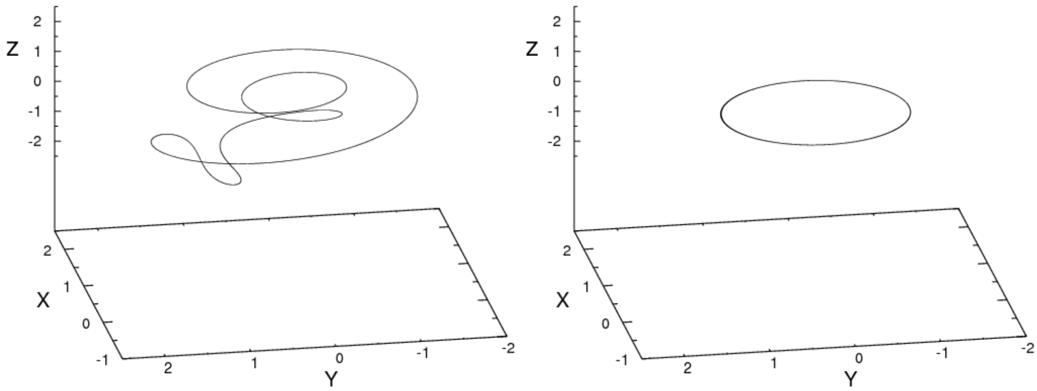

(a) IC 1 (b) IC 2

Figure 4.3: The L84 model attractor when $F = 6$, illustrated using a single model realisation over a simulation period of 1 year with ICs: (a) $(X, Y, Z) = (0.12, 0.95, -0.26)$ and (b) $(X, Y, Z) = (0.93, -1.04, 0.58)$.

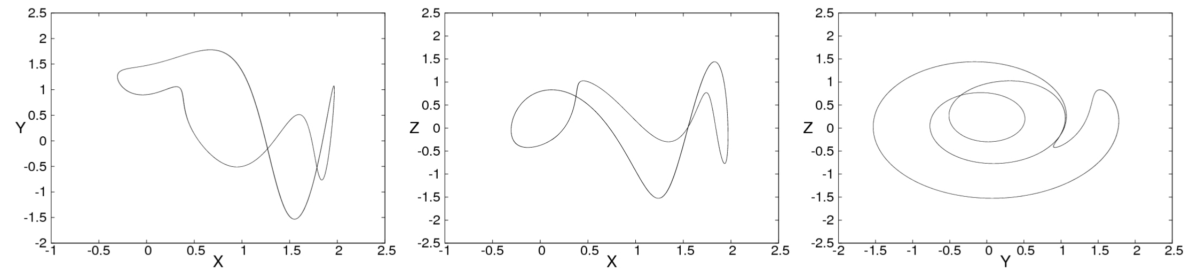

(a) X-Y Plane, IC 1 (b) X-Z Plane, IC 1 (c) Y-Z Plane, IC 1

Figure 4.4: The L84 model attractor in the X-Y, X-Z and Y-Z planes when $F = 6$, illustrated using a single model realisation over a simulation period of 1 year with ICs: $(X, Y, Z) = (0.12, 0.95, -0.26)$.

Figures 4.3(a) and 4.3(b) show the evolution of two single model trajectories orbiting the L84 attractor with summer parameter values ($F = 6$) from two different initial states: *IC 1* $(0.12, 0.95, -0.26)$ and *IC 2* $(0.93, -1.04, 0.58)$. The two initial states were specifically chosen to depict the two coexisting attractors, referred to as $A1$ for figure 4.3(a) and $A2$ for figure

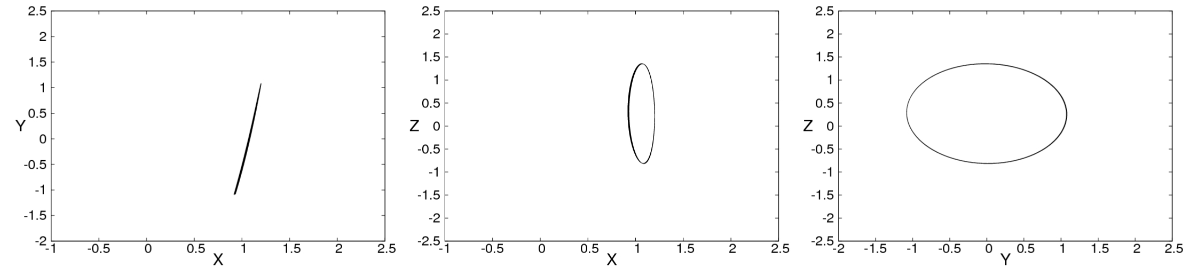

(a) X-Y Plane, IC 2 (b) X-Z Plane, IC 2 (c) Y-Z Plane, IC 2

Figure 4.5: The L84 model attractor in the X-Y, X-Z and Y-Z planes when $F = 6$, illustrated using a single model realisation over a simulation period of 1 year with ICs: $(X, Y, Z) = (0.93, -1.04, 0.58)$.

4.3(b). In both examples the attractors no longer exhibit chaotic behaviour but rather display periodicity. Attractor $A1$ (associated with *IC 1*) is shown in three dimensions in figure 4.3(a) and in two dimensions in figures 4.4(a) to 4.4(c). The plots reveal that the attractor occupies similar ranges in each model variable to those observed when $F = 8$. The attractor is composed of predominantly westerly winds which spiral away from the origin with a regular transition to easterly flow.

The alternative attractor $A2$ (associated with *IC 2*), shown in three dimensions in figure 4.3(b) and in two dimensions in figures 4.5(a) to 4.5(c), reveals a much simpler geometric shape; an ellipse which is almost parallel to the Y-Z plane. The strength of the westerly winds are constrained to values between $0.9 < X < 1.2$ and the periodicity is highly regular.

The coexistence of two attractors for the same parameter values indicates sensitivity of the attractor itself to the initial model state; not to be confused with chaotic sensitivity to the initial state when $F = 8$. As stated by Lorenz (1990), the attractors in the summer configuration display intransitive behaviour where the climates, once established, will persist forever. The presence of intransitivity and coexisting attractors has implications when considering the predictability of the climate from an uncertain initial state. Clearly IC uncertainty is a primary concern when predicting the evolution of any dynamical system which does not have a unique attractor.

A basin of attraction can be defined as the set of ICs in the model/system state space for which trajectories evolve towards a certain attractor (Aguirre et al. (2003)). To illustrate the nature of the basins of attraction in the summer configuration of the L84 model, a large IC ensemble is run and the attractors to which the model trajectories evolve over time are identified for each ensemble member. The plot in figure 4.6 shows the results of a 1,000,000 member ensemble run (1,000 by 1,000 grid resolution), for an array of ICs spread evenly from $(-1.0, -2.5, 0)$ to $(2.5, 2.5, 0)$, after a 20 year model simulation (a lower resolution version is provided in the Lorenz (1990) study). The results show the basins of attraction in the X-Y plane, where $Z = 0$.

Figure 4.6 shows that for the IC ensemble selected, the majority of ensemble members propagate

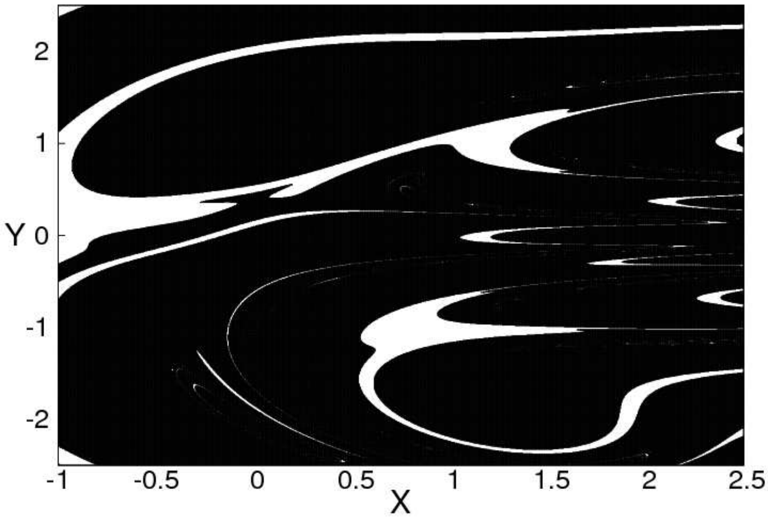

Figure 4.6: The basins of attraction in the X-Y plane where $Z = 0$ for ICs in the L84 model when $F = 6$. The black area denotes the basin of attraction for $A1$ and the white area the basin of attraction for $A2$. The image resolution is 1,000 by 1,000 points equivalent to 1 mega-pixel.

towards $A1$. The regions of model state space in which ICs propagate towards the alternative attractor $A2$ are relatively narrow and meander within the basin of attraction for $A1$. The boundaries between the basins of attraction are smooth and the separations appear distinct. However the limited resolution may obscure regions of model state space which are more intricate on finer resolutions. The overall image reveals a complicated terrain with fine structure and narrow separation between basin's of attraction in certain regions of the model state space where the attractor to which a trajectory propagates is highly sensitive to the precision of the initial model state.

It is suggested in the paper by Freire et al. (2008) that for certain parameter values the basins of attraction for the L84 model display evidence of the "Wada" property. The existence of such a property means that the attractor to which a model trajectory evolves is not only highly sensitive to the initial state but that, when there exist at least three basins, an individual basin's boundary belongs simultaneously to the boundary of the other two (or more) basins (Aguirre et al. (2003)). In permanent summer, when $F = 6$, only two attractors have been found to coexist so the Wada property cannot exist. However, a seasonal cycle is introduced in section 4.4 and the model becomes exposed to regions of parameter space that exhibit the Wada property. The implications of the exposure of model trajectories to such regions are discussed further in section 4.6.

4.3 L84 Climates

4.3.1 Single trajectory results

Adopting the same approach as that applied to the analysis of the L63 model, the climate of the L84 model is first investigated by running a single model realisation and determining the time scale over which the frequency distributions converge. The model is initialised at the three different states used to generate the figures in section 4.2 and each model realisation is integrated for a period of 100 years. The frequency distributions for the X variable of the model trajectories are given in figures 4.7 to 4.9 (Y and Z variable distributions given in figures B-1 to B-6 in Appendix B). The bin width used to generate the frequency distribution plots in this chapter is 0.01, unless stated otherwise. Each single trajectory distribution consists of every model state through which the trajectory passes during the simulation period. For longer simulation periods, the number of points included in the frequency distributions therefore increases.

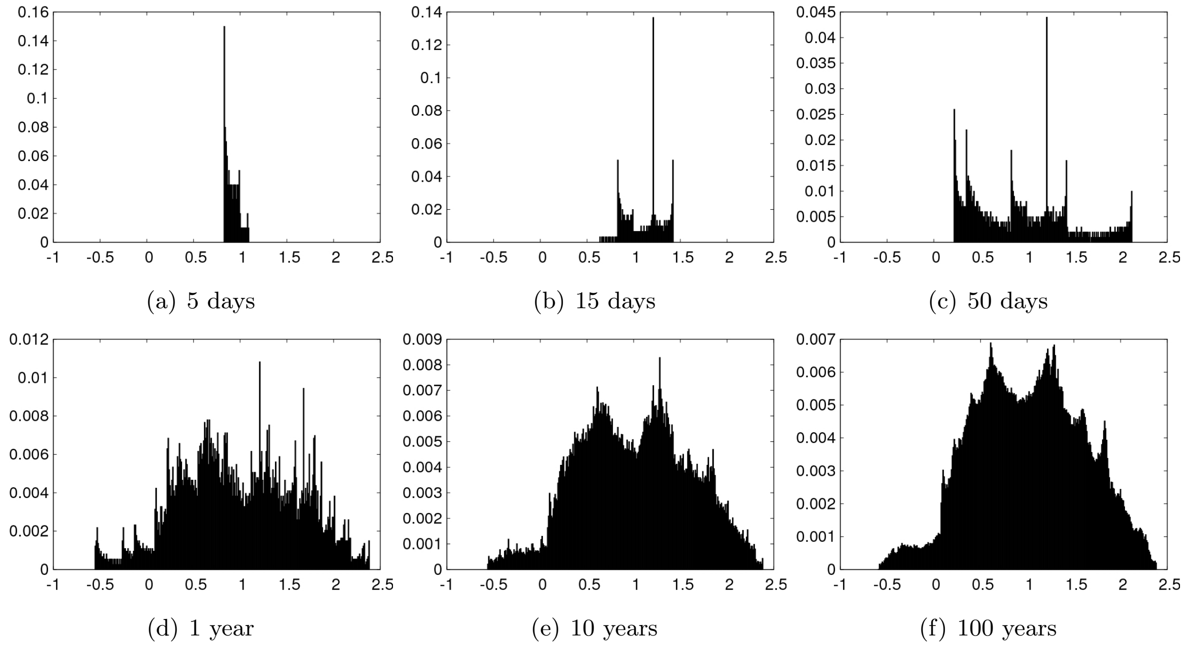

(a) 5 days (b) 15 days (c) 50 days

(d) 1 year (e) 10 years (f) 100 years

Figure 4.7: Normalised frequency distributions of the X variable for a single trajectory in the L84 model when $F = 8$ after given simulation periods, with ICs: $(X, Y, Z) = (1.0, 1.0, 1.0)$. In each plot, the x-axis denotes the X variable and the y-axis corresponds to the frequency per occupied bin; bin width = 0.01. Y and Z variable distributions given in Appendix B: figures B-1 and B-2.

The plots in figure 4.7 show the normalised frequency distributions when $F = 8$ (permanent winter conditions) for simulation periods of 5 days up to 100 years. The results show that a number of orbits are required before the range of the attractor is fully explored. Even after 50 days, the negative X (easterly) regime is not visited for the model trajectory shown. In figures 4.7(d) to 4.7(f), the majority of the distribution's density is in the positive X (westerly) regime. The 10 and 100 year distributions reveal two peaks at approximately $X = 0.6$ and $X = 1.3$ and

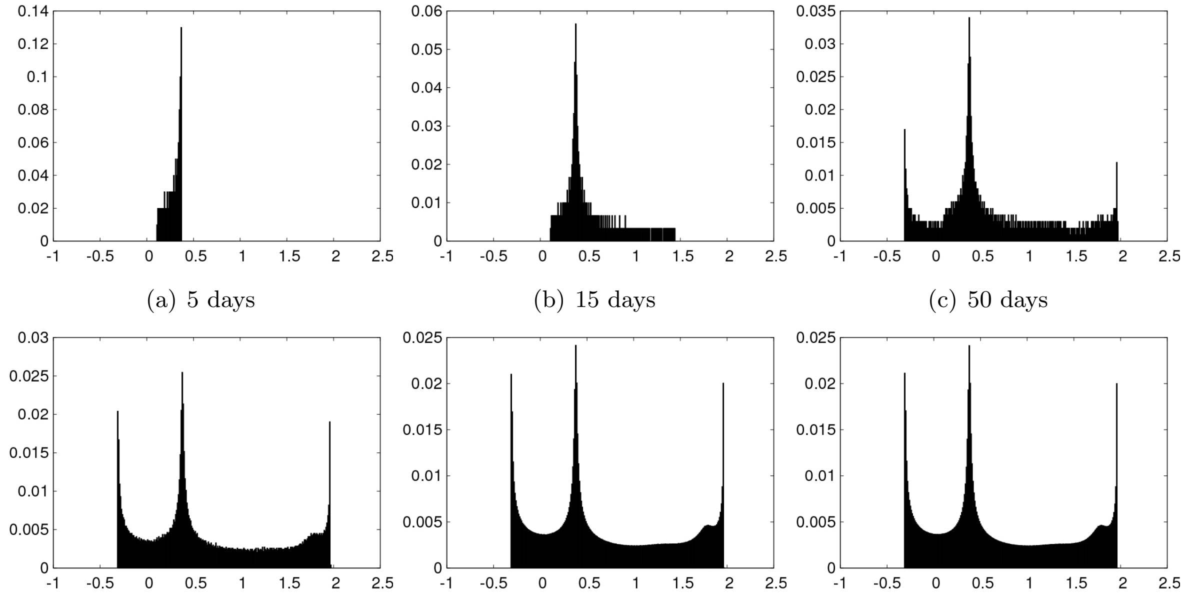

(a) 5 days (b) 15 days (c) 50 days

(d) 1 year (e) 10 years (f) 100 years

Figure 4.8: Normalised frequency distributions of the X variable for a single trajectory in the L84 model when $F = 6$ after given simulation periods, for *IC 1*: $(0.12, 0.95, -0.26)$. In each plot, the x-axis denotes the X variable and the y-axis corresponds to the frequency per occupied bin; bin width $= 0.01$. Y and Z variable distributions given in Appendix B: figures B-3 and B-4.

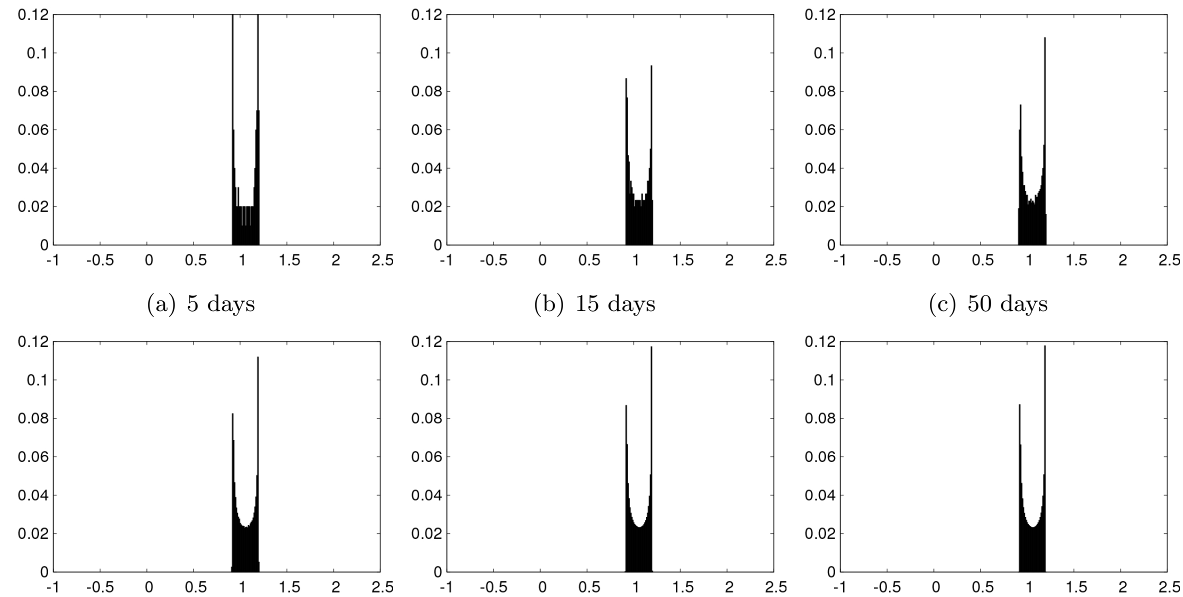

(a) 5 days (b) 15 days (c) 50 days

(d) 1 year (e) 10 years (f) 100 years

Figure 4.9: Normalised frequency distributions of the X variable for a single trajectory in the L84 model when $F = 6$ after given simulation periods, for *IC 2*: $(0.93, -1.04, 0.58)$. In each plot, the x-axis denotes the X variable and the y-axis corresponds to the frequency per occupied bin; bin width $= 0.01$. Y and Z variable distributions given in Appendix B: figures B-5 and B-6.

a range of X values that extends between $-0.6 < X < 2.4$.

Figure 4.8 and 4.9 show the normalised frequency distributions for two single trajectories, initialised at *IC 1* and *IC 2* respectively, for permanent summer conditions over simulation periods of 5 days up to 100 years. The results show that the time required for a trajectory to explore the range of model states on attractor $A2$ is longer than the time it takes to visit the complete range of states on attractor $A1$. In figure 4.9, the full range of X values is sampled after only 5 days (see fig. 4.9(a)), largely as a result of the simple geometric nature of the attractor $A2$; an ellipse consisting of periodic orbits on the time scale of approximately one time unit (equivalent to 5 days). However, as shown in figure 4.8(c), it takes 50 days before the frequency distribution begins to visually resemble the distributions associated with longer model simulations. In general, the model climate distributions are much smoother under summer parameter conditions for both ICs because of the periodic nature of the model attractors.

4.3.2 Ensemble results

The climate distributions of the L84 model with fixed parameter values are also estimated for permanent summer and permanent winter conditions using an IC ensemble approach. Large IC ensembles (10,000 members) are run for simulation periods of up to 100 years with ICs spread along a transect in the model state space; from $(-1.0, -2.5, -2.5)$ to $(2.5, 2.5, 2.5)$. Figure 4.10 shows the evolution of the IC ensemble frequency distributions for the X variable at particular time instants during permanent winter conditions. The distributions appear to converge after approximately one year; after 50 days the distribution retains significant memory of the ICs with some members still located outside of the range of X values consistent with the model attractor.

As expected, from experience with the L63 model, convergence of the distributions is more rapid using the IC ensemble approach. Visual inspection suggests that the ergodic assumption is valid in the winter configuration, as the converged distribution resembles the single trajectory distribution shown in figure 4.7(f); a quantitative analysis is employed in section 4.3.3 using the KS test.

The equivalent plots for permanent summer conditions are displayed in figure 4.11. After one year, the range of X values becomes well constrained and matches the range associated with the single trajectory distributions shown in figure 4.8, associated with attractor $A1$. The location of the peaks in the distributions shown in figures 4.11(d) to 4.11(f) are broadly consistent with the five peaks identified in figures 4.8 and 4.9 indicating that the two coexisting attractors illustrated in section 4.2.3 are both prevalent in the ensemble frequency distributions. However, because the ensemble distributions do not match the single trajectory distributions for both *IC 1* and *IC 2*, the ergodic assumption does not appear to be valid in permanent summer conditions. Furthermore, at the time instants chosen, the ensemble distributions have not converged as some of the peaks are inconsistent in magnitude. In permanent summer conditions, the model is not

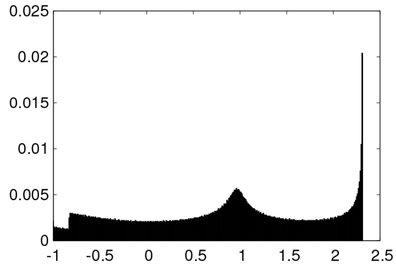

(a) 5 days

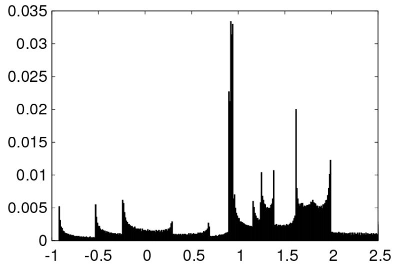

(b) 15 days

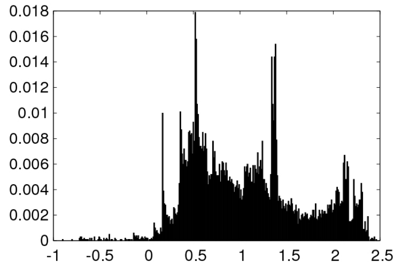

(c) 50 days

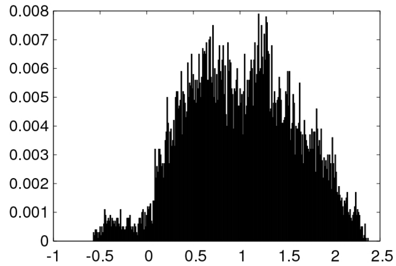

(d) 1 year

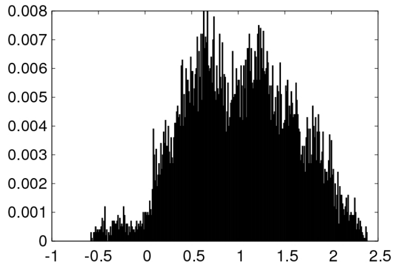

(e) 10 years

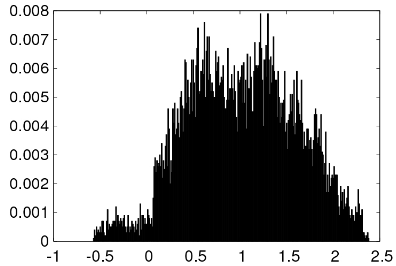

(f) 100 years

Figure 4.10: Normalised frequency distributions for a 10,000 member IC ensemble of the L84 model when $F = 8$ after given simulation periods with ICs spread along a transect from $(-1.0, -2.5, -2.5)$ to $(2.5, 2.5, 2.5)$. In each plot, the x-axis denotes the X variable and the y-axis corresponds to the frequency per occupied bin; bin width = 0.01. Y and Z variable distributions given in Appendix B: figures B-7 and B-8.

chaotic and the model trajectories display periodicity. As a result the ensemble distributions (at a specific instant in time) show the distribution of model states at a specific phase of each trajectory's periodic cycle so the distribution is, and always will be, conditioned on the ICs in the ensemble.

Analysis of four different IC ensemble distributions evolving over a 80 year simulation period shows that under permanent summer conditions IC ensemble distributions are different at every instant in the model simulation and that the distributions are conditioned on the IC uncertainty encapsulated in the IC ensemble. Figure 4.12 shows frequency distributions from four different ensembles (labelled $E1$, $E2$, $E3$ and $E4$) at regular intervals over a 80 year simulation period. The ICs for the ensembles are chosen with reference to the basins of attraction (shown in figure 4.6) in the X-Y plane, where $Z = 0$, and the ranges are listed in table 4.1. For each ensemble, the ICs are uniformly distributed within the specified ranges. Ensembles $E1$ and $E2$ are selected for regions in which all trajectories evolve to attractor $A1$ and attractor $A2$ respectively. Ensembles $E3$ and $E4$ are selected in other regions of the model state space which span both basins of attraction.

Figures 4.12(a) to 4.12(d) show the initial uniform spread of the IC ensembles in the X variable for each ensemble. The plots in the first two columns of figure 4.12 show the $E1$ and $E2$ distributions at 20 year intervals over the 80 year simulation period. The distributions are constrained to the ranges in the model variables associated with their respective attractors.

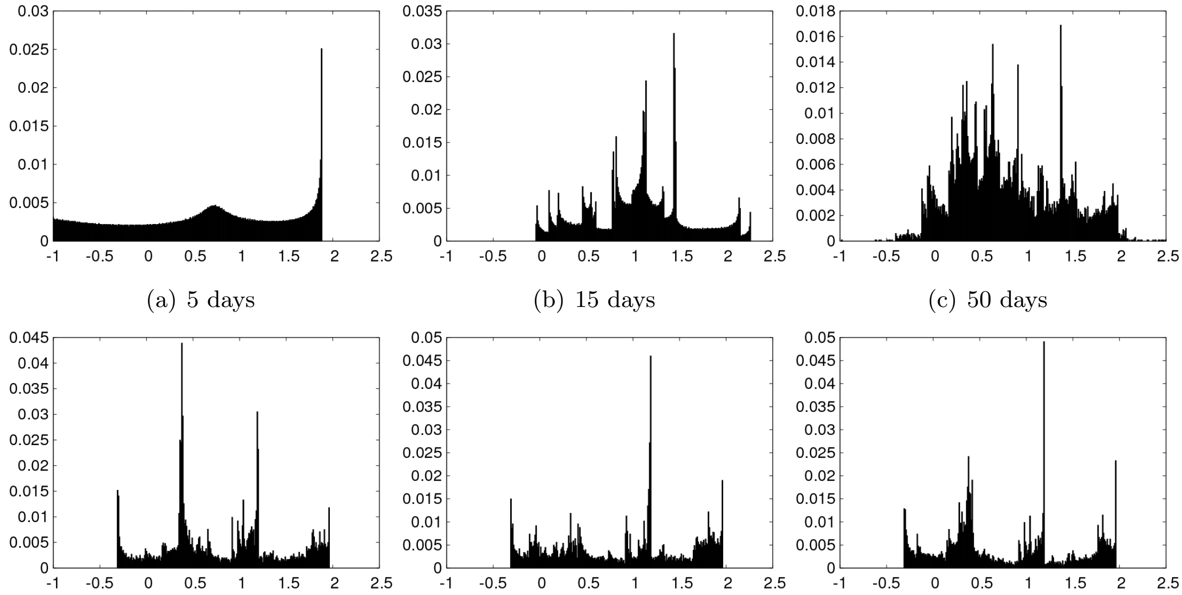

(a) 5 days (b) 15 days (c) 50 days

(d) 1 year (e) 10 years (f) 100 years

Figure 4.11: Normalised frequency distributions for a 10,000 member IC ensemble of the L84 model when $F = 6$ after given simulation periods with ICs spread along a transect from $(-1.0, -2.5, -2.5)$ to $(2.5, 2.5, 2.5)$. In each plot, the x-axis denotes the X variable and the y-axis corresponds to the frequency per occupied bin; bin width = 0.01. Y and Z variable distributions given in Appendix B: figures B-9 and B-10.

Ensemble	X_{min}	X_{max}	Y_{min}	Y_{max}
$E1$	-1.0	-0.5	-1.5	-1.0
$E2$	-1.0	-0.8	0.0	0.3
$E3$	1.0	1.5	1.0	1.5
$E4$	-0.5	0.0	0.0	0.5

Table 4.1: IC ranges for four different ensembles used to investigate memory in the L84 model for permanent summer conditions, when $F = 6$.

The plots in columns three and four show the distributions associated with $E3$ and $E4$. The results show that when the IC ensemble crosses the boundaries in the basins of attraction, some members evolve on attractor $A1$ and others evolve on attractor $A2$, as evident in the locations of the primary peaks consistent with $A2$ and the location of other members in the state space consistent with $A1$. The distributions are also different at each time instant for each ensemble supporting the inference that periodicity controls the evolution of the model trajectories. Because the model is not chaotic, trajectories do not separate from each other so the distributions continue to exhibit memory of the ICs and do not converge. In section 4.3.3, the convergence of both single trajectory and IC ensemble distributions is quantitatively assessed using the KS test and the results support the notion that IC memory is apparent in the ensemble distributions under permanent summer conditions.

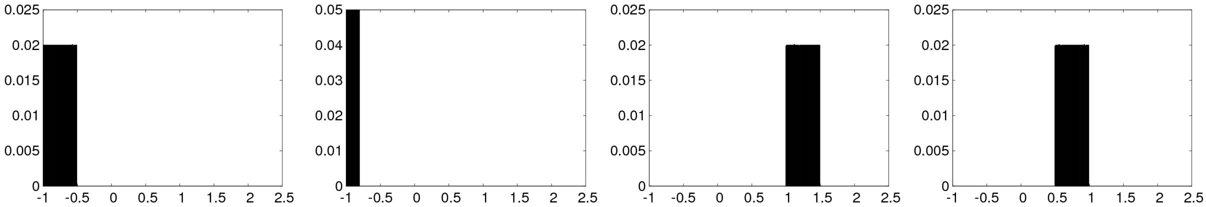

(a) E1, 0 years (b) E2, 0 years (c) E3, 0 years (d) E4, 0 years

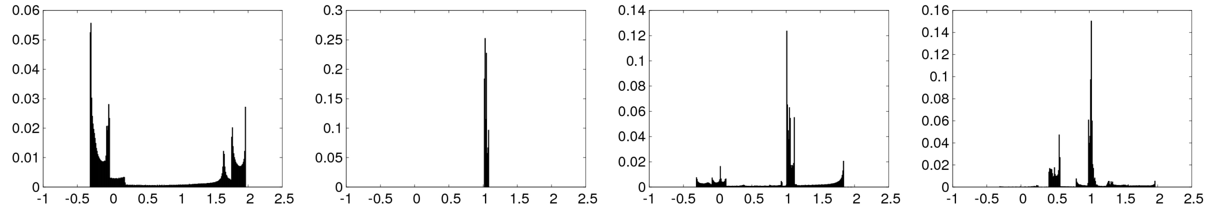

(e) E1, 20 years (f) E2, 20 years (g) E3, 20 years (h) E4, 20 years

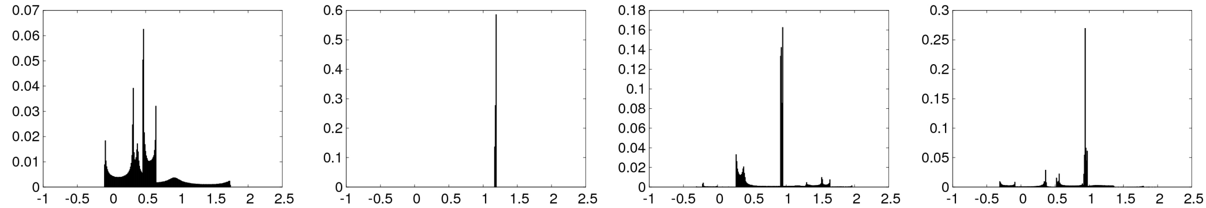

(i) E1, 40 years (j) E2, 40 years (k) E3, 40 years (l) E4, 40 years

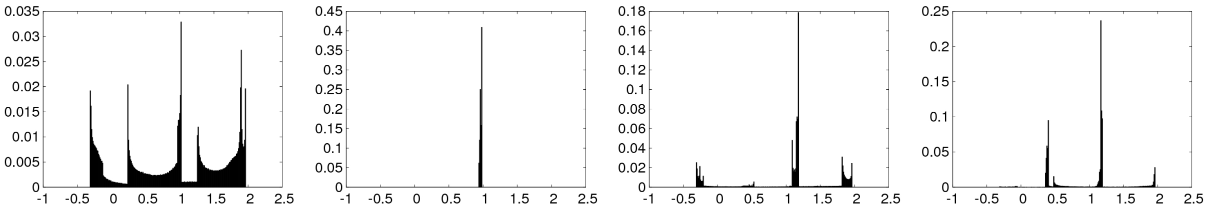

(m) E1, 60 years (n) E2, 60 years (o) E3, 60 years (p) E4, 60 years

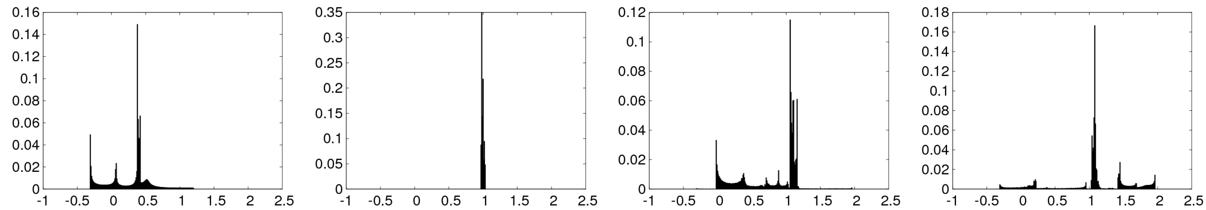

(q) E1, 80 years (r) E2, 80 years (s) E3, 80 years (t) E4, 80 years

Figure 4.12: Normalised frequency distributions of four different 10,000 member IC ensembles for the X variable in L84 model in permanent summer conditions ($F = 6$). The first column shows the distributions for ensemble E1, the second column shows the distributions for ensemble E2, the third column shows the distributions for ensemble E3 and the fourth column shows the distributions for ensemble E4. In each plot, the x-axis denotes the X variable and the y-axis corresponds to the frequency per occupied bin; bin width = 0.01.

Sensitivity to model time step

In section 3.3.5, the L63 model climate distributions are shown to be sensitive to the model time step. To test the sensitivity of the L84 model to the chosen time step, a series of model runs are performed. Lorenz (1984) used a time step $\tau = \frac{1}{30}$, albeit with a fourth order Taylor-series integration procedure, whilst in this study a smaller time step $\tau = 0.01$ is implemented using a fourth order RK integration method. Figure 4.13 shows the distribution in X from a 100 year run of a 10,000 member IC ensemble for four different time steps of decreasing size. The ICs used are the same as those used to generate figures 4.10 and 4.11; a transect from $(-1.0, -2.5, -2.5)$ to $(2.5, 2.5, 2.5)$. The results indicate that the time step used is an important consideration in determining the climate distributions of the L84 model. For time steps of $\tau \leq 0.01$, the distributions are very similar but when $\tau = \frac{1}{30}$ the climate distribution is significantly altered. Over reasonably short times scales (years to decades), when $\tau = \frac{1}{30}$ the L84 model displays chaotic behaviour but over longer time scales (multi-decadal to centennial) model trajectories become periodic and affect the ensemble climate distributions. Figure 4.14 illustrates the transition from chaotic to periodic behaviour, shown for the X variable for a 50 year simulation of the L84 model with a time step, $\tau = \frac{1}{30}$. Whilst the truncation effect resulting from the time step choice on model climates has been observed in the L63 model (Teixeira et al. (2007)), at the time of writing (to the author's knowledge) no such acknowledgement regarding the sensitivity of the L84 model climate to the time step has been published in the formal literature. Based on these results, a time step of $\tau = 0.01$ using the fourth order RK method was deemed appropriate for the L84 experiments presented in this thesis.

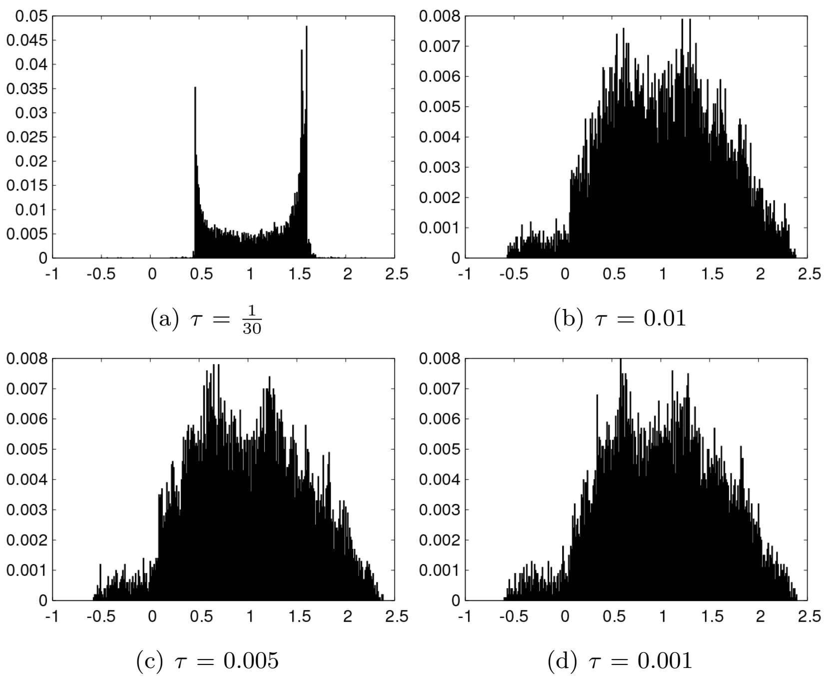

(a) $\tau = \frac{1}{30}$ (b) $\tau = 0.01$

(c) $\tau = 0.005$ (d) $\tau = 0.001$

Figure 4.13: 10,000 member IC ensemble normalised frequency distributions for the L84 model when $F = 8$ after an integration period of 100 years for given time steps, using a fourth order RK integration scheme and ICs spread along a transect from $(-1.0, -2.5, -2.5)$ to $(2.5, 2.5, 2.5)$. In each plot, the x-axis denotes the X variable and the y-axis corresponds to the frequency per occupied bin; bin width = 0.01.

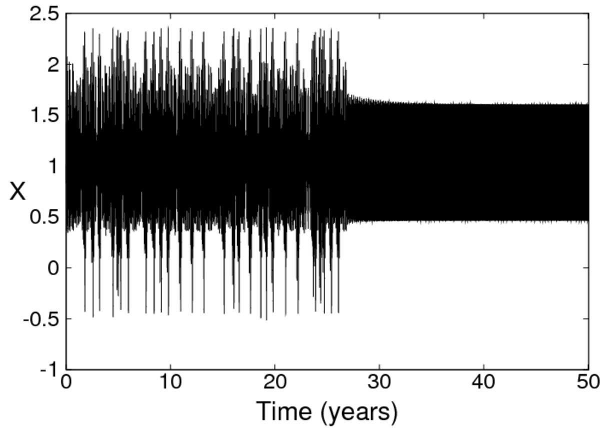

Figure 4.14: Single model trajectory for the variable X in the L84 model after a 50 year simulation with $\tau = \frac{1}{30}$ and IC: $(X, Y, Z) = (1.0, 1.0, 1.0)$.

4.3.3 Rates of convergence for model climate distributions in the L84 model

In order to estimate the time scales at which the distributions from single model trajectories and IC ensembles converge to the climate distributions of the L84 model, a very large IC ensemble (100,000 members) is run to provide benchmark ensemble climate distributions for the L84 model in permanent winter and permanent summer parameter conditions. The ensemble is run for a period of 200 years with ICs spread along a transect from $(-1.0, -2.5, 2.5)$ to $(2.5, 2.5, 2.5)$. A period of 200 years is chosen to ensure that model trajectories evolve many times around the model's attractor(s).

Using the KS test, the corresponding benchmark ensemble distributions (shown in figure 4.15) are compared to the single trajectory distributions from section 4.3.1 and the 10,000 member IC ensemble distributions described in section 4.3.2. The corresponding KS plots for permanent winter and permanent summer parameter conditions are shown in figures 4.16 and 4.17 respectively.

When $F = 8$ (permanent winter), the L84 model displays chaotic transitive behaviour and over time the trajectories spread out across the attractor state space. The KS plots in figure 4.16 reveal the rate at which memory of the initial state(s), of a single trajectory and an IC ensemble, are lost as the distributions converge towards the benchmark ensemble distributions. After only one and a half months, D decreases to values close to $D = 0.1$ in both the single trajectory and ensemble distributions. After one year the IC ensemble appears to have largely converged towards the model climate distributions whereas the single trajectory distributions retain some memory of the initial state for approximately ten years.

The KS plots in figure 4.17 show that the initial rates of convergence for permanent summer conditions are similar to those for permanent winter conditions but crucially, both of the single trajectory distributions and the ensemble distributions do not entirely converge towards the benchmark ensemble distributions (consistent with the results in section 4.3.2). Given the

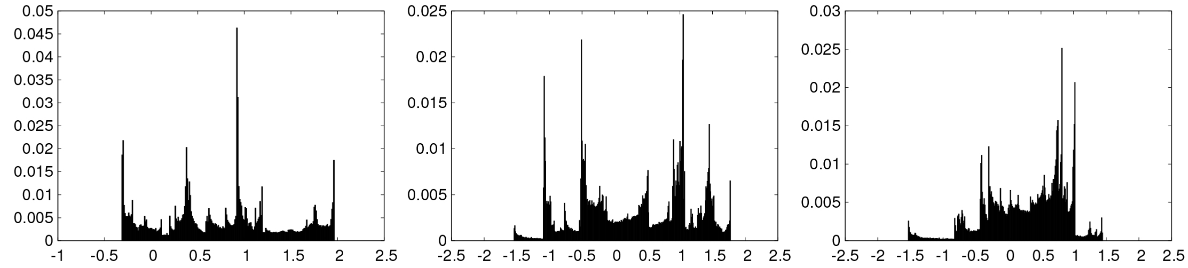

(a) X, summer (b) Y, summer (c) Z, summer

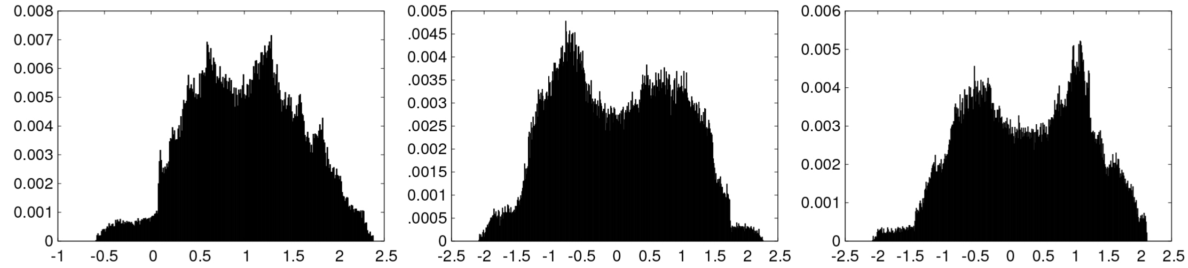

(d) X, winter (e) Y, winter (f) Z, winter

Figure 4.15: Normalised frequency distributions for given variables in permanent summer, (a) to (c), and permanent winter, (d) to (f), after a 200 year simulation of the L84 model from a 100,000 member IC ensemble with ICs spread along a transect from $(-1.0, -2.5, 2.5)$ to $(2.5, 2.5, 2.5)$. In each plot, the y-axis corresponds to the frequency per occupied bin; bin width = 0.01.

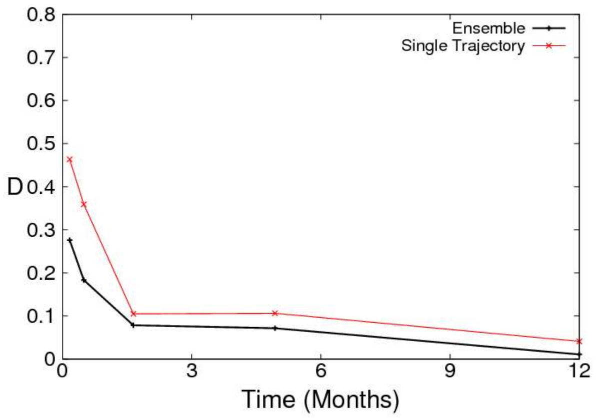

(a) 1 year

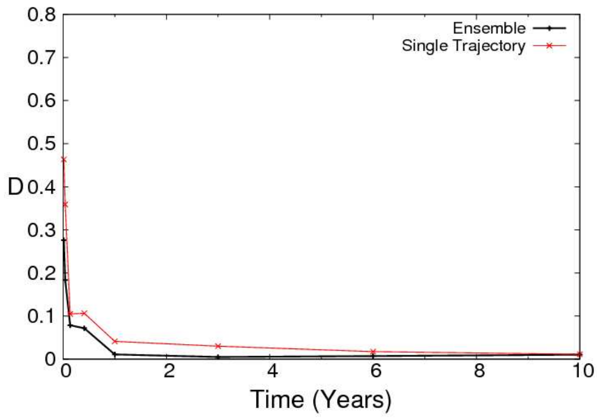

(b) 10 years

Figure 4.16: KS comparisons for the X variable in the L84 model when $F = 8$ between the 100,000 member IC ensemble distributions shown in figure 4.15 and: (i) the 10,000 member IC ensemble distributions shown in figure 4.10; and (ii) the single trajectory distributions shown in figure 4.7. Y and Z variable KS comparisons shown in Appendix B, figures B-11 and B-12.

intransitive nature of the model when $F = 6$, it is not surprising that the single trajectory distributions do not converge to the benchmark ensemble distributions. The distributions from the trajectory associated with $A1$ converge more than those associated with $A2$, as the range of behaviour of model trajectories evolving on $A1$ is consistent with the range of the ensemble

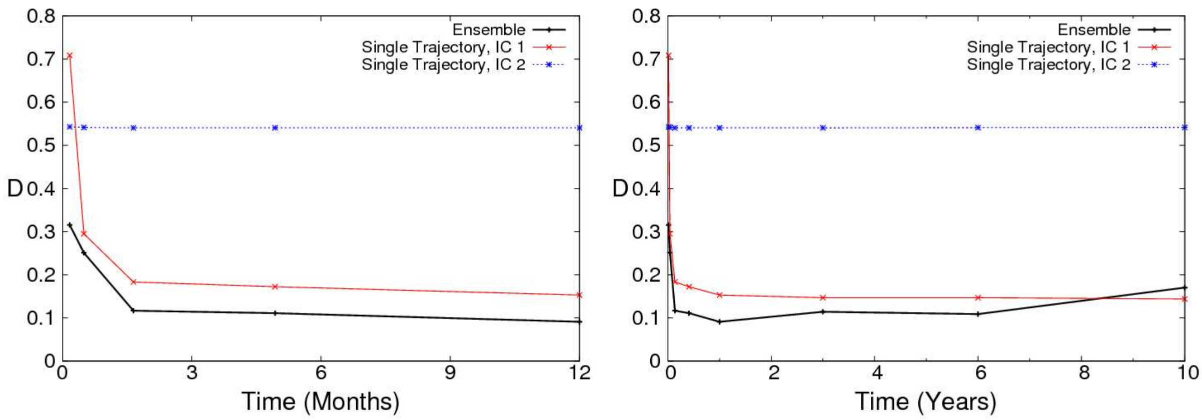

(a) 1 year (b) 10 years

Figure 4.17: KS comparisons for the X variable in the L84 model when $F = 6$ between the 100,000 member IC ensemble distributions shown in figure 4.15 and: (i) the 10,000 member IC ensemble distributions shown in figure 4.11; (ii) the single trajectory distributions shown in figure 4.8 from $IC1$ (associated with attractor $A1$); and (iii) the single trajectory distributions shown in figure 4.9 from $IC2$ (associated with attractor $A2$). Y and Z variable KS comparisons shown in Appendix B, figures B-13 and B-14.

distributions, and more ensemble members are likely to evolve on $A1$ based on evidence from their basins of attraction (see figure 4.6).

The KS results confirm that over the 10 year period shown in figure 4.17(b) the ensembles also retain memory of their ICs as the ensemble distributions do not fully converge. Figure B-15 in appendix B shows that the distributions similarly fail to converge over a much longer simulation period of 160 years. The ergodic assumption is therefore invalid for permanent summer conditions, where the model behaviour is intransitive. In the L84 model, when $F = 6$, two climates coexist and the long-term climate which is realised is dictated entirely by the model's initial state. If this initial state is uncertain then an IC ensemble will generate the PDFs of the model variables for some future time conditioned on the IC uncertainty.

In the analogy to climate prediction under IC uncertainty, if the uncertainty in the initial state of the climate system crosses the boundaries of the basins of attraction of at least two coexisting attractors then using an IC ensemble is essential to determine what states are possible in the future. If two (or more) climates coexisted and the uncertainty in the initial state of the climate system encompasses more than one basin of attraction then running an IC ensemble to determine possible future states would be vitally important in guiding robust adaptation strategies. Deriving the distribution of climate using a single model trajectory from a single initial state would be misleading.

4.4 Seasonally Driven L84 Model

A number of studies have explored the dynamics of the seasonally driven L84 model documenting the associated phenomenology and linking the results to interannual climate variability (Lorenz (1990), Kock (1998), Broer et al. (2002) and Broer et al. (2003)). The seasonality has usually been introduced into the modelling studies by imposing a periodic (sinusoidal) variation in the equator-to-pole temperature difference, F. Broer et al. (2002) also impose a seasonal cycle on the land-ocean temperature contrast, G, but for the purposes of this study G shall be held constant, consistent with the methodology adopted by Lorenz (1990). The focus of the work presented in this section and the following section is to investigate how a seasonal cycle in F can impact the L84 model climate distributions, with and without a trend in the model parameter, and to relate the L84 model results to the real climate system in terms of understanding the potential predictability of climate under climate change.

4.4.1 Single trajectory under seasonal variations in F

To implement a seasonal cycle in the L84 model, the value of F in equation 4.1 is replaced by the sinusoidal function given in equation 4.4:

$$F \to F_m + M\cos\left((2\pi \frac{i}{K\tau^{-1}}) - \frac{\pi}{12}\right) \tag{4.4}$$

where F_m is the mean value of F, τ is the model time step, i is the iteration step number, K denotes the number of time units per year and the term $\frac{\pi}{12}$ is introduced to ensure that the time series in F begins each phase on January 1st, half a month before the maximum value of F is reached (to align a model year with a calendar year). M represents the magnitude of the wave so that in the case where $M = 1$, and $F_m = 7$, the seasonal fluctuations are contained in the range: $6 < F < 8$. The parameter space contains a diverse set of chaotic and non-chaotic attractors (Freire et al. (2008)) exhibiting both transitive and intransitive behaviour. Lorenz (1990) states "intransitive behaviour occurs nearly everywhere between $F = 5.2$ and 6.9 while transitive chaotic behaviour occupies the interval from 7.9 to 8.8. Between 6.9 and 7.6, transitivity prevails, with only weak periodic fluctuations, while between 7.6 and 7.9 intransitivity reappears, with weak periodic or strong chaotic variations." Crucially, Lorenz notes that these findings only correspond to fixed value of F.

Figure 4.18 shows the evolution of a single model trajectory for each model variable over a 10 year simulation of the seasonally driven L84 model where $F_m = 7$ and $M = 1$. The plots show interannual variability in the summer and winter circulation patterns. In the third, fourth, fifth, seventh and final year of the simulation, periodicity which spans the range of the model state space is apparent during the summer months. The remaining summers are associated with constrained periodic oscillations, particularly evident in the X variable. Lorenz (1990) refers to these summers as strong and weak respectively. In the winter months, the trajectory appears to

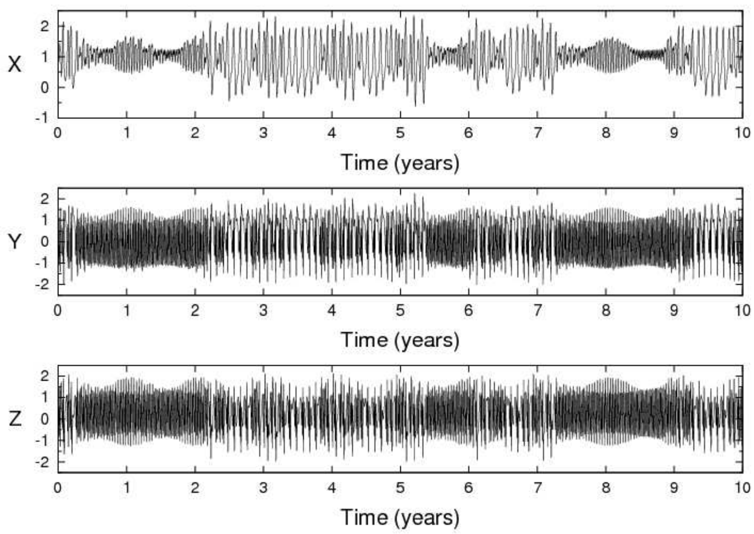

Figure 4.18: Time series' for model variables from a single trajectory simulation of the seasonally driven L84 model over a 10 year interval initiated on January 1st with ICs: $(X, Y, Z) = (1.0, 1.0, 1.0)$. $F_m = 7$, $M = 1$.

be less regular but at $t = 1$ year and $t = 8$ years there is evidence of periodicity in the months leading to mid-winter. The dynamics of the seasonally driven L84 model has been relatively well studied for single model trajectories (Lorenz (1990), Broer et al. (2002)). In the analogy to the climate system and climate prediction the focus of the remainder of this chapter is on the model climate distributions which haven't (to the author's knowledge) been researched in any detail. In the next section, the climate distributions of the seasonally driven L84 model are determined.

Although model trajectories strictly evolve according to different attractors at different fixed values of F, the effect of a seasonal cycle is to create a new "pseudo-attractor" on which trajectories propagate. Whilst the term has been used for other purposes elsewhere in the literature (e.g. Burns et al. (1993)), here the term *pseudo-attractor* (PA) is used to describe the geometric nature of the attractor as it evolves in time in accordance with the periodic variations in F. The term pseudo-attractor is subsequently used throughout the remainder of this chapter to distinguish it from an autonomous attractor at fixed parameter values.

4.4.2 Seasonally driven L84 model climate distributions

The conventional approach to assessing climate variability using a single model realisation is compared to the IC ensemble approach in the seasonally driven L84 model. A 100,000 member IC ensemble, with ICs spread along a transect from $(-1.0, -2.5, 2.5)$ to $(2.5, 2.5, 2.5)$, is run for a period of 200 years to estimate the equilibrium climate distributions of the seasonally driven L84 model for mid-winter (when F returns to $F = 8$) and mid-summer (when F returns to $F = 6$). The frequency distributions for the three model variables at mid-winter and mid-summer (in the 200th simulation year) are shown in figure 4.19.

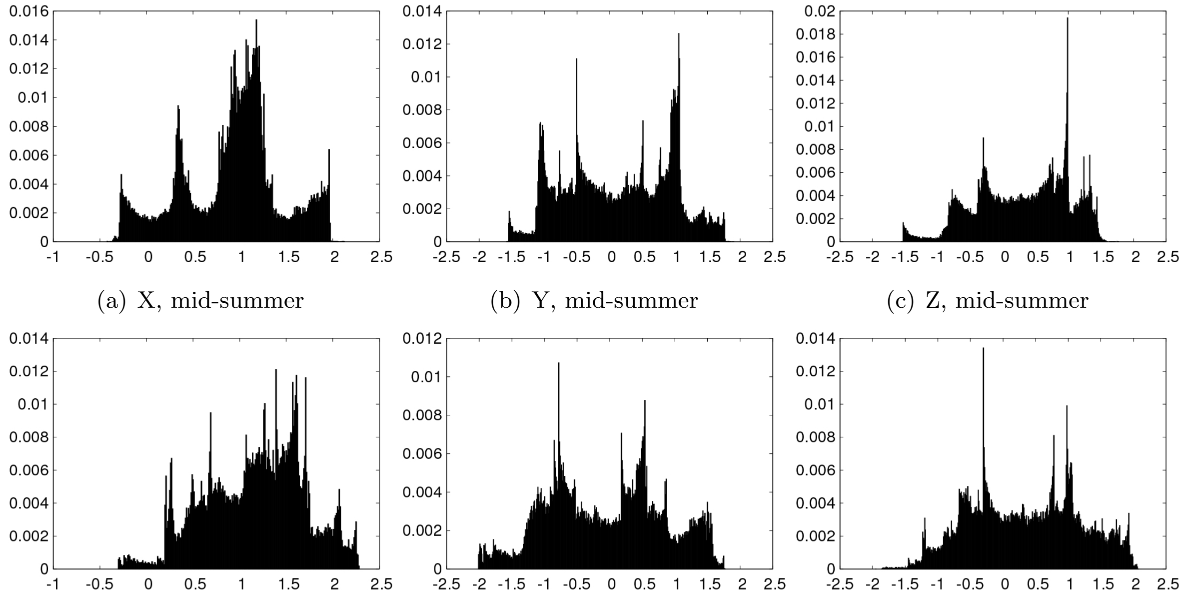

(a) X, mid-summer (b) Y, mid-summer (c) Z, mid-summer

(d) X, mid-winter (e) Y, mid-winter (f) Z, mid-winter

Figure 4.19: Normalised frequency distributions for given variables in mid-summer, (a) to (c), and mid-winter, (d) to (f), after a 200 year simulation of the seasonally driven L84 model with $F_m = 7$ and $M = 1$ from a 100,000 member IC ensemble with ICs spread along a transect from $(-1.0, -2.5, 2.5)$ to $(2.5, 2.5, 2.5)$. In each plot, the y-axis corresponds to the frequency per occupied bin; bin width $= 0.01$.

The distributions in figure 4.19 are different to the equivalent plots in the non-seasonally driven L84 model, shown in figure 4.15. Whilst the range in model behaviour remains consistent across all variables, the density of the trajectories in given regions of the PA state space is altered. For example, during permanent summer in the non-seasonally driven model (figure 4.15(a)), there is a narrow peak at $X \approx 0.9$. Yet in the seasonally driven model (figure 4.19(a)), the summer distribution shows a much wider peak in this region of state space, with a more uniform modal range of trajectories occurring between $0.8 < X < 1.2$. Similarly, during permanent winter in the non-seasonally driven model (figure 4.15(d)), there is a high density of values in the range $0.5 < X < 1.5$. In the seasonally driven model during mid-winter (figure 4.19(d)), there remains a high density of trajectories where $1.0 < X < 1.5$ but there is a smaller density in the range $0.5 < X < 1.0$.

The seasonal cycle in F significantly influences the probabilities of trajectories passing through certain regions of the model state space. The seasonal cycle imposes transitions from regions of parameter space with chaotic attractors, associated with transitive behaviour, to regions with multiple periodic attractors, associated with intransitive behaviour. Model trajectories are constantly adjusting to the changing geometry of the underlying model attractor(s). Trajectories retain memory of previous states associated with different regions of parameter space which exhibit alternative long-term dynamic behaviour. The ensemble 'climate' distributions shown in figure 4.19 therefore seem to be exhibiting hysteresis; a memory of the pathway in F.

4.4.3 Testing the ergodic assumption

The ergodicity of the seasonally driven L84 model is explored for both mid-summer and mid-winter forcing conditions. Given the inference that the seasonally driven L84 model displays transitive behaviour, one would expect the ergodic assumption to be valid for a sufficiently long single model realisation. However, determining the length of time required for single model distributions to converge towards the ensemble distributions at specific times in the year (e.g. mid-winter/mid-summer) is not a trivial calculation.

A single model realisation is run for 10,000 years with ICs $(1.0, 1.0, 1.0)$ initiated on January 1st. The single trajectory distributions are then derived from the distribution of yearly recurring values for mid-winter (when F returns to $F = 8$) and mid-summer (when F returns to $F = 6$). Only one model state is extracted per year for both mid-winter and mid-summer; hence a 10 year sample includes 10 data points. Each value can be considered independent from the previous years value as chaotic conditions in the preceding winter lead to rapid deviations of model trajectories[2]; as discussed in section 4.2.1, Lorenz (1990) demonstrated that the summertime circulation is effectively randomly selected due to chaotic conditions in the previous winter circulation.

Figure 4.20 shows the distribution for mid-summer values of X from a single trajectory integrated over increasing time periods. As the model simulation period increases, the frequency distributions appear to be converging towards the ensemble distribution displayed in figure 4.19(a); a quantitative comparison is provided in figure 4.22. For shorter simulation periods, the distributions are inevitably less detailed given that only one state is selected per year. After 30 years, a time scale typically associated with climate definitions (Burroughs (2003)), the range of possible states is reasonably well captured but the density of values is not sufficient to provide reliable estimates of the model probabilities. After 100 years and certainly by 300 years, some important features of the distributions become more apparent but quantitative estimates of the entire model PDF are likely to contain inaccuracies.

The equivalent distributions for the mid-winter values of X are shown in figure 4.21. The 10,000 year distribution, shown in figure 4.21(h), visually appears to closely resemble the ensemble distribution for mid-winter X given in figure 4.19(a). Consistent with figure 4.20, shorter time intervals provide less representative estimates of the model climate distributions. Unlike in figure 4.20(c), the 30 year distribution shown in figure 4.21(c) does not fully capture the range of X values associated with the mid-winter ensemble distribution. Crucially the distribution does not include any values of X that are negative, which represent transitions to easterly flow. The density of points is also different with a primary cluster of points close to $X = 0.6$; a region with a relatively lower probability of occurring in larger samples.

[2]For a comparative analysis of the error growth in both the L63 and L84 models, see Anderson and Hubeny (1997).

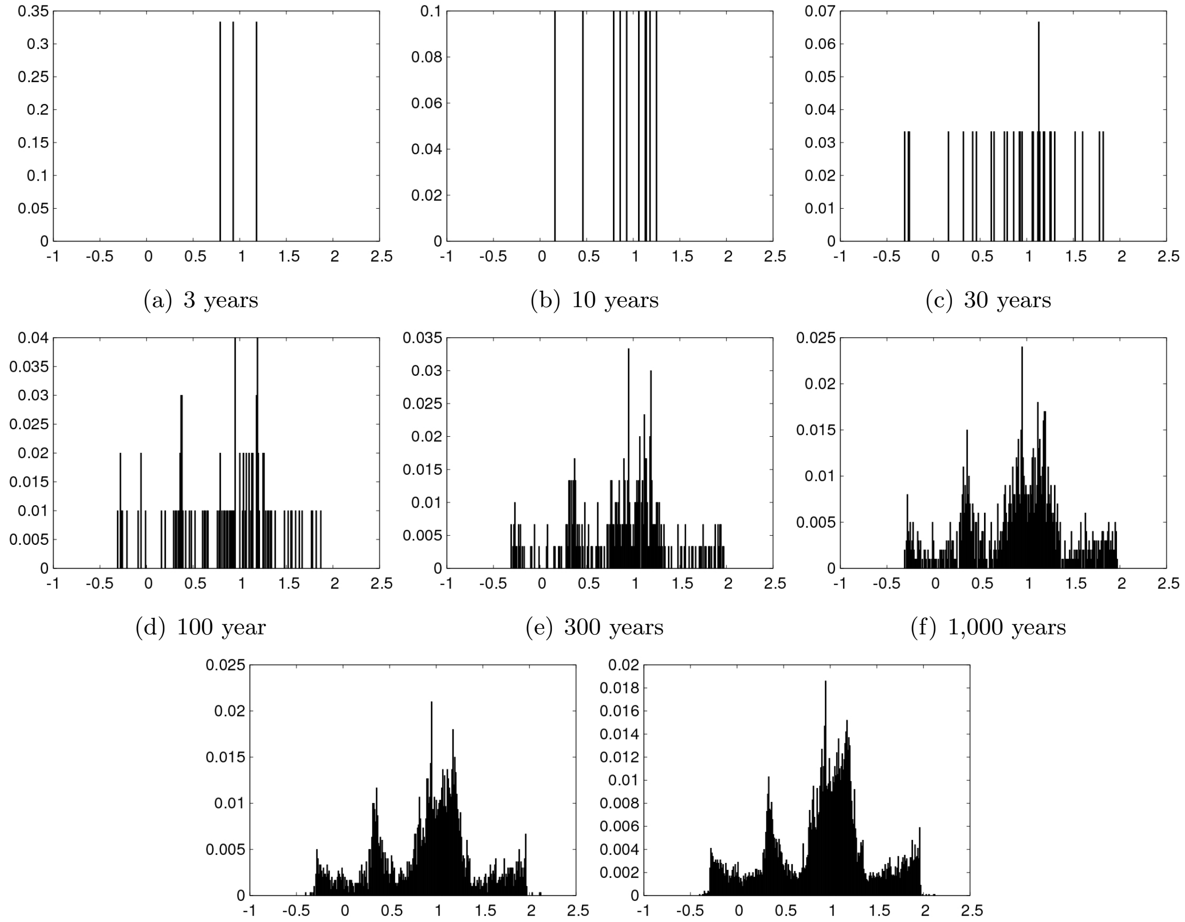

(a) 3 years (b) 10 years (c) 30 years

(d) 100 year (e) 300 years (f) 1,000 years

(g) 3,000 years (h) 10,000 years

Figure 4.20: Normalised frequency distributions of the X variable for a single trajectory in the L84 model in mid-summer after given simulation periods with seasonal F variations between $6 < F < 8$ and ICs: $(X, Y, Z) = (1.0, 1.0, 1.0)$. In each plot, the x-axis denotes the X variable and the y-axis corresponds to the frequency per occupied bin; bin width $= 0.01$.

Using the KS test, the large IC ensemble distributions, representing the climate of the seasonally driven L84 model (shown in figure 4.19), are compared to the single trajectory distributions of increasing simulation periods (shown in figures 4.20 and 4.21). Time series' of D comparing the single trajectory distributions to the ensemble distributions are displayed in figure 4.22. The x-axis has a logarithmic scale from 1 to 10,000 years. The results reveal, unsurprisingly, that the longer the integration period for a single model realisation the lower the value of D (corresponding to a better fit).

The convergence illustrated in figure 4.22 is simply a function of an increasing number of data-points in the single trajectory distributions. Increasing the number of data-points, by including data at time steps close to mid-summer or mid-winter, might therefore appear to be a possible solution to estimating the model climate in a more computationally efficient manner. However, this approach is problematic. The parameter F and the associated model attractor(s)

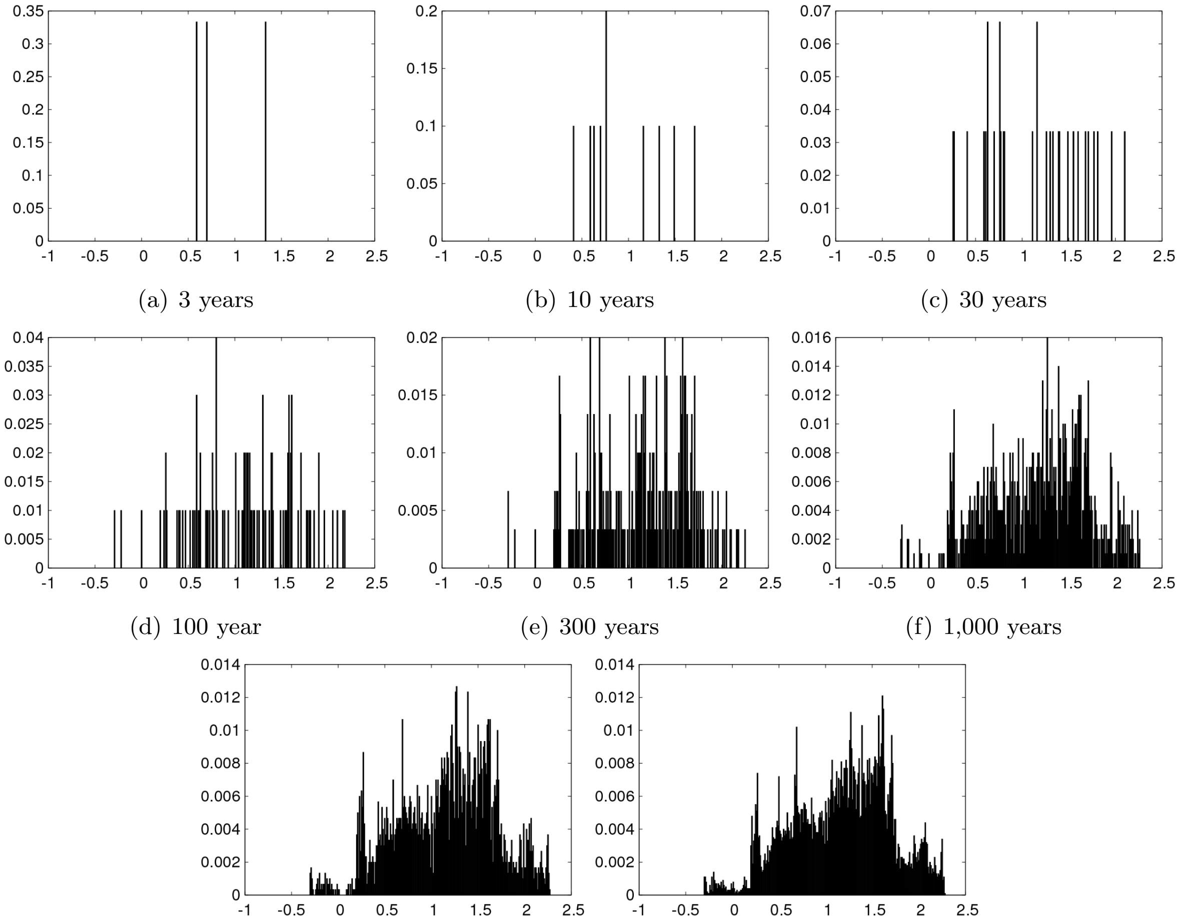

(a) 3 years (b) 10 years (c) 30 years

(d) 100 year (e) 300 years (f) 1,000 years

(g) 3,000 years (h) 10,000 years

Figure 4.21: Normalised frequency distributions of the X variable for a single trajectory in the L84 model in mid-winter after given simulation periods with seasonal F variations between $6 < F < 8$ and ICs: $(X, Y, Z) = (1.0, 1.0, 1.0)$. In each plot, the x-axis denotes the X variable and the y-axis corresponds to the frequency per occupied bin; bin width $= 0.01$.

is continuously changing throughout the year so using data points from time steps close to but not at the time of interest risks including data points that are potentially associated with a different attractor. The impact of increasing the sample size is investigated and the results are described in the following section.

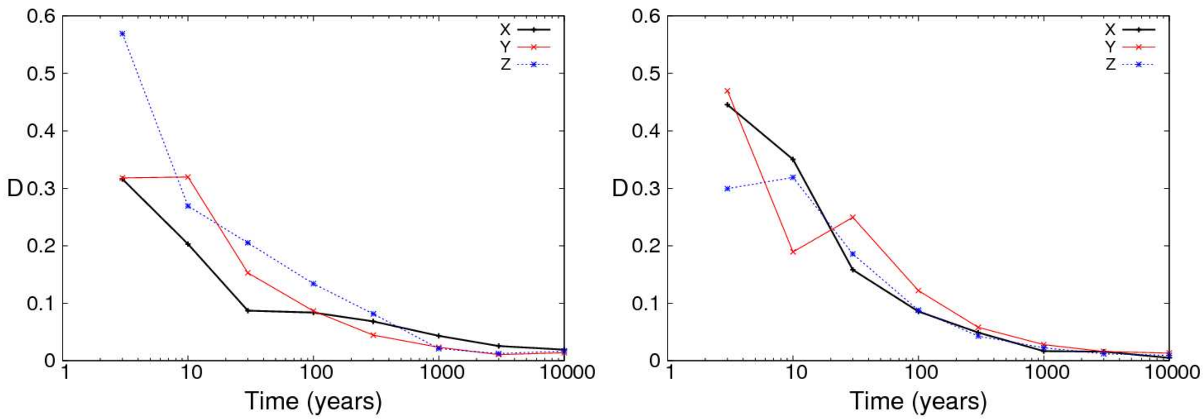

(a) Summer (b) Winter

Figure 4.22: KS comparison between single trajectory distributions and 100,000 member IC ensemble climate distributions for the seasonally driven L84 model. The single trajectory distributions consist of one model state per year extracted at mid-winter and mid-summer. The ensemble distributions are also extracted at mid-winter and mid-summer.

4.4.4 Increasing the sample size

With a time scale of 5 days and a time step, $\tau = 0.01$, the number of data-points in the L84 model year is 7300 (equivalent to the number of time-units per year ($\frac{365}{5}$) divided by the time step). Rather than selecting a single data point for each consecutive mid-winter/mid-summer, all of the January/July data points are selected, thus increasing the number of data points per year for a single model realisation by a factor of 608[3]. The value of F at the beginning and end of January is $F = 7.966$; only 0.034 K less than the mid-winter value of $F = 8$. Similarly, the value of F at the beginning and end of July is $F = 6.034$; only 0.034 K greater than the mid-summer value of $F = 6$. One might therefore expect that by including all of the January/July data points, the frequency distributions of mid-winter/mid-summer resulting from a single model trajectory should converge towards the IC ensemble distributions more rapidly.

Figure 4.23 show the KS comparison of the single trajectory distributions with monthly data to the IC ensemble distributions shown in figure 4.19. The KS plots show that the single trajectory distributions do indeed converge to the ensemble distributions more rapidly when including all of the monthly data points (note the y-axis is the same scale as that used in figure 4.22). Even after the first year, the KS result conveys a moderate level of agreement. However the distributions never converge entirely and the values of D remain significantly larger than zero, even over a long simulation period of 1,000 years (which includes 608,000 data points). D does not decrease any further after a time interval of approximately 10 years in both mid-winter and mid-summer, suggesting that longer simulation periods do not necessarily lead to better agreement in the distributions.

The most significant differences between the single trajectory distributions and the ensemble

[3]The number of data points in an individual month is therefore 608.

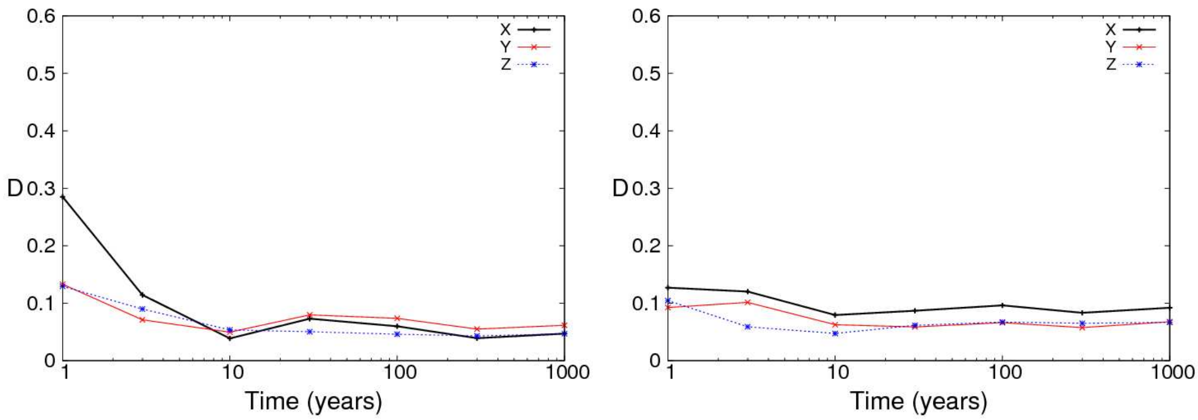

(a) Mid-summer

(b) Mid-winter

Figure 4.23: KS comparison between single trajectory distributions and IC ensemble climate distributions for the seasonally driven L84 model. Data taken from the entirety of January and July for the single trajectory distributions whilst ensemble distributions are extracted at mid-winter and mid-summer respectively.

distributions appears in the X variable in winter, where the KS statistic converges to $D \approx 0.1$. Figures 4.24(a) to 4.24(c) show the frequency distributions associated with consecutive January values of X from 100, 300 and 1,000 year simulation periods and figure 4.24(d) shows the 200 year ensemble distribution of mid-January X values, also illustrated in figure 4.19(d). The distributions from the single model trajectory shown in figures 4.24(a) to 4.24(c) appear to have converged toward a stable distribution that is different from the ensemble distribution shown in figure 4.24(d). There is a small difference in the range of X values; the mid-winter ensemble distribution suggests a slightly narrower range, $-0.3 < X < 2.3$, as opposed to the single trajectory approach using data from the whole of January which suggests a range of $-0.4 < X < 2.4$. However the most significant difference is in the density of values in the region close to $X = 0.6$. The single model realisations show distributions with high densities of values in the regions close to $X = 0.6$ and $X = 1.3$. The ensemble result reveals a comparatively less dense region near $X = 0.6$ with more ensemble members in the region close to $X = 1.3$.

Using data which is not consistent with the underlying forcings, as a pragmatic solution to limited computational capacity, is potentially misleading. Utilising model data points that are close in time to the interval of interest can yield inaccurate information about the statistical properties of a particular variable's climate distributions. Such discrepancies may be less obvious for a system which is not subject to complex changes in the behaviour of attractors associated with the system forcings but high-dimensional systems, such as the climate system, are unlikely to exhibit less complex behaviour than the highly idealised model considered here. The results demonstrated using the L84 model have implications for climate modelling relating to the interpretation of probabilistic estimates based on temporally averaged data in addition to those already discussed in relation to the ergodic assumption. These potential implications are discussed further in section 4.6.

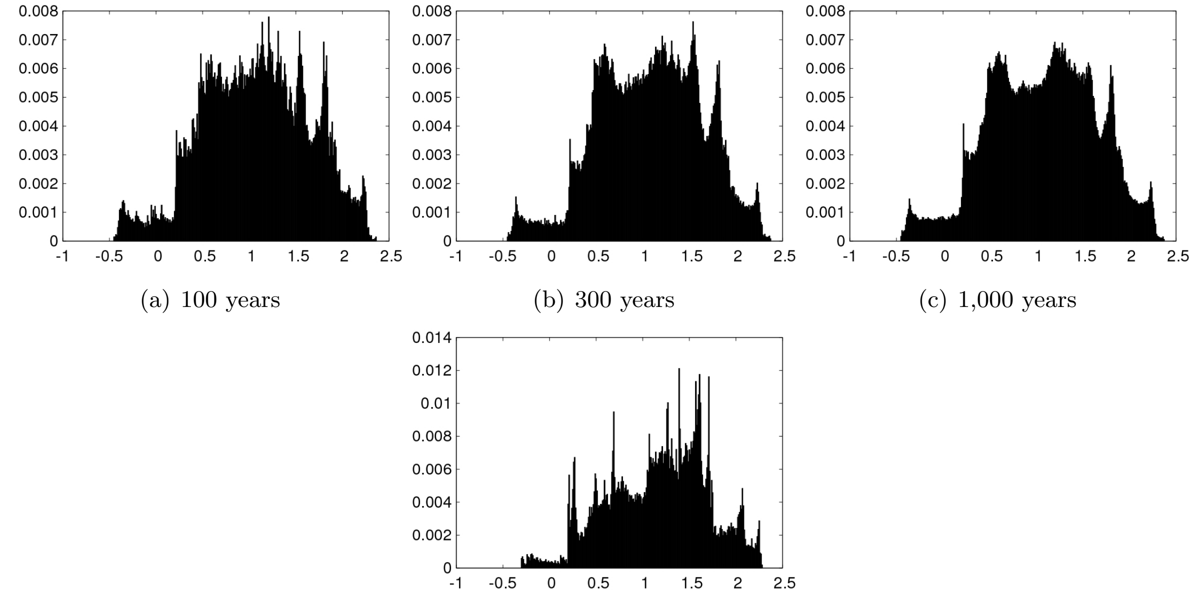

(a) 100 years (b) 300 years (c) 1,000 years

(d) Ensemble from fig. 4.19(d)

Figure 4.24: Normalised frequency distributions of the X variable for a single trajectory of the L84 model for consecutive month's of January after given simulation periods, (a) to (c), and a 100,000 member ensemble after 200 years (d), with seasonal F variations between $6 < F < 8$ and ICs: $(X, Y, Z) = (1.0, 1.0, 1.0)$. In each plot, the x-axis denotes the X variable and the y-axis corresponds to the frequency per occupied bin; bin width = 0.01.

The results presented in this section suggest that long multi-centennial simulations of a single model trajectory are required to establish a distribution of model states that accurately represents the climate distribution at a specific time of the year, given a seasonal variation in a key model parameter. Short sampling periods of a single model trajectory are unable to capture some of the large scale features of the IC ensemble distributions. Over longer simulation periods the number of sample points increases to provide improved estimates of the model's climate in both of the seasons investigated and the use of the ergodic assumption becomes less problematic.

For a number of variables in the climate system, even in the absence of long-term trends in the climate forcings, it seems likely that the distribution of system states will have irregular properties due to the numerous modes of internal variability which can affect atmospheric and oceanic circulation patterns on all spatial scales. Therefore, even if ergodicity is considered to be a valid assumption for the system over very long time scales, experiments with the L84 model suggest that a short sampling period of observations or model projection data may provide misleading estimates of the climate variable distributions associated with a particular forcing scenario.

When using climate models to investigate climate variability at a given spatial scale for decadal and multi-decadal predictions, long-term global and regional trends need to be acknowledged in both the design phase of modelling experiments and in communicating the model output to the user community. In extending the analogy, the next section presents an analysis of the behaviour of the seasonally driven L84 model when subject to trends in the parameter F.

4.5 Introducing Trends into the L84 Model

Climate model projections support theoretical reasoning that as the world warms in response to anthropogenic emissions of GHGs, high latitude regions will warm at a faster rate than equatorial regions (Collins and Senior (2002), Masson-Delmotte et al. (2006)). As a consequence the average equator-to-pole temperature difference will decrease. In the L84 model, F represents the meridional temperature difference and in the seasonally driven L84 model, the value of F decreases in the summer. Consequently, introducing a trend towards lower values of F, as an analogy to the impact of global warming on the equator-to-pole temperature difference, will manifest itself in a change towards a more "summer-like" parameter configuration. Whilst no direct quantitative comparison can be made between the behaviour of the L84 model and the real climate system, understanding the impact of trends in the L84 model may yield qualitative insight into the predictability of the climate under climate change. Hence there is no *correct* specification for the magnitude and pathway of a trend in F to represent the GHG-induced radiative forcing. A number of different trends were therefore considered but the results of the L84 experiments presented here focus on a linearly decreasing trend in F.

4.5.1 Linear decrease in F

To introduce a linear trend in the parameter F, in the seasonally driven L84 model, another term is added to equation 4.4 so that F varies according to equation 4.5:

$$F \to F_m + M \cos\left((2\pi \frac{i}{K\tau^{-1}}) - \frac{\pi}{12}\right) + H \frac{i}{K\tau^{-1}} \tag{4.5}$$

where H is the average increase (or decrease when negative) in F per year and the other variables take the values given in section 4.4.

The time series of F, shown in figure 4.25, is applied to the L84 model. The oscillations during the first 30 years of the period remain unchanged but after 30 years, a linear decreasing trend is imposed where $H = -0.0\dot{2}$ (a decrease in F of 1 unit every 45 years) so that the mean value of F decreases from $F_m = 7$ to $F_m = 6$ at 75 years into the model simulation. The magnitude of the seasonal cycle is kept constant throughout the simulation period.

The ergodic assumption is examined for the L84 model with a linear trend in F. A large IC ensemble is run subject to the trend in F illustrated in figure 4.25. The 10,000 ensemble members are selected at the end of a 100 year ensemble run of the seasonally driven L84 model; the original 10,000 ensemble members were initiated from points along the transect described in section 4.3.2. The ICs generated span the range of the ensemble distributions that occur on January 1^{st}, where $F = 7.966$. The ICs that are used for the ensemble runs are displayed in figure 4.26.

Maintaining the focus on the mid-summer and mid-winter climates, the states of the IC ensemble members are examined in both mid-summer and mid-winter every 15 years over the 90 year

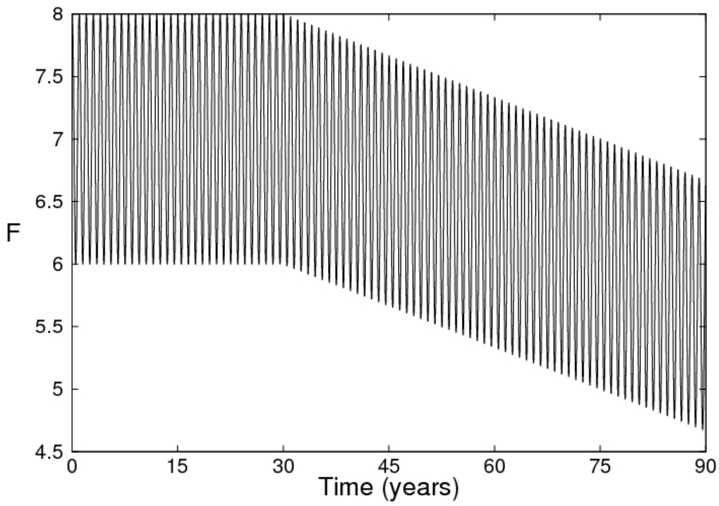

Figure 4.25: Time series in F over 90 year period with a linear decrease in F beginning after 30 years with a rate $H = -0.0\dot{2}$.

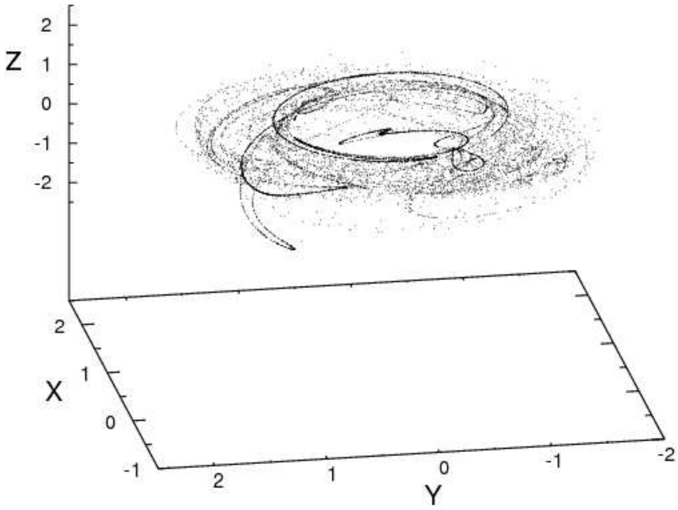

Figure 4.26: 10,000 ICs used for the ensemble model runs in section 4.5. Extracted from the output of a 100 year run of the seasonally driven L84 model with ICs originating from points spread evenly along a transect in the model state space from $(-1.0, -2.5, -2.5)$ to $(2.5, 2.5, 2.5)$

period (i.e. ensemble distributions observed at 15, 30...90 years). A single model trajectory is also run for the 90 year period and the state of the trajectory at each consecutive mid-summer and mid-winter time step is extracted. The IC ensemble frequency distributions taken at 15 yearly intervals are compared to the distribution of states from a 30 year sample of the single model trajectory, centred on the 15 yearly time instants. The results reveal the extent to which single model trajectory distributions capture the statistics of the IC ensemble distributions and support (or oppose) the ergodic hypothesis under a changing climate. Figure 4.27 shows the temporal evolution of the IC ensembles and the single trajectory distributions.

The left column of figure 4.27 shows the IC ensemble distributions at given years in the

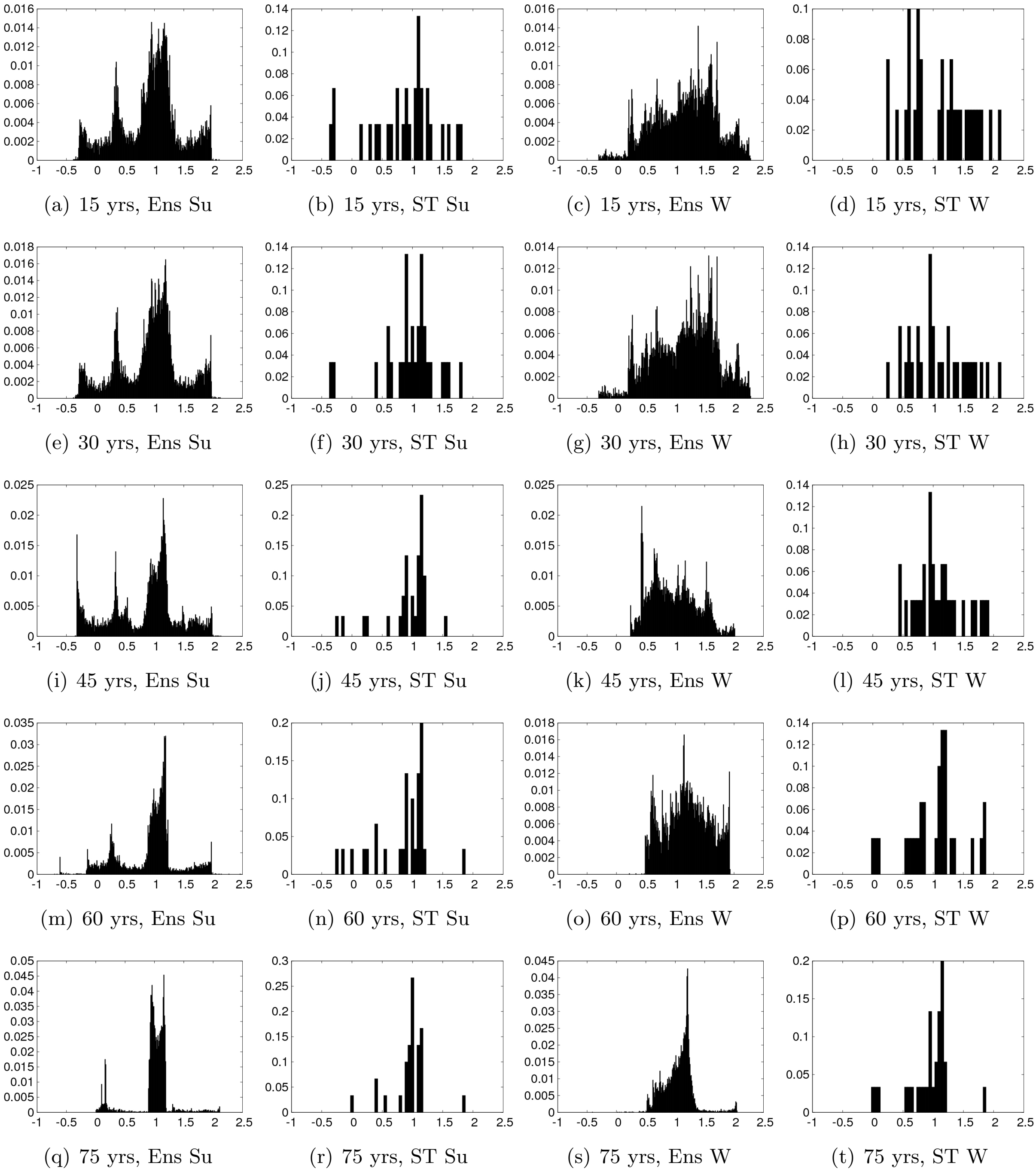

(a) 15 yrs, Ens Su (b) 15 yrs, ST Su (c) 15 yrs, Ens W (d) 15 yrs, ST W

(e) 30 yrs, Ens Su (f) 30 yrs, ST Su (g) 30 yrs, Ens W (h) 30 yrs, ST W

(i) 45 yrs, Ens Su (j) 45 yrs, ST Su (k) 45 yrs, Ens W (l) 45 yrs, ST W

(m) 60 yrs, Ens Su (n) 60 yrs, ST Su (o) 60 yrs, Ens W (p) 60 yrs, ST W

(q) 75 yrs, Ens Su (r) 75 yrs, ST Su (s) 75 yrs, Ens W (t) 75 yrs, ST W

Figure 4.27: IC ensemble and single trajectory normalised frequency distributions for the X variable in the seasonally driven L84 model when subject to a decreasing trend in F with $H = -0.0\dot{2}$. The first and third columns show the 10,000 member IC ensemble frequency distributions (Ens) after given time instants for mid-summer (Su) and mid-winter (W) respectively. The second and fourth columns show the equivalent distributions from 30 year samples centred on given time instants of a single model realisation (ST) initiating from $(1.0, 1.0, 1.0)$ in mid-summer and mid-winter respectively. In each plot, the x-axis denotes the X variable and the y-axis corresponds to the frequency per occupied bin; bin width = 0.01 for the ensemble distributions; bin width = 0.05 for the single trajectory distributions.

simulation period at mid-summer. In panels (a) and (e), the distributions are similar, which is unsurprising given that there is no trend in F during the first 30 years of the model simulation; the distributions therefore approximate the climate distribution of the seasonally driven L84 model in the X variable in mid-summer. Over time the value of F decreases, as shown in figure 4.25, and the ensemble distributions respond. The density of trajectories in the region close to $X = 1$ increases at the expense of the other regions illustrated in the subsequent plots shown in panels (i), (m) and (q). The second column shows the equivalent climate distribution estimates from 30 year samples of a single model trajectory centred on the given time instants. The distribution in panel (b) captures the range of X values reasonably well and shows a greater density in the modal region at $X = 1$, apparent in panel (a). However, due to the irregular nature of the climate distribution, a sample of 30 data points is too small to capture many of the key features of the ensemble distributions such as the secondary modal peaks. In panel (f), the single trajectory distribution suggests an increase in the probability of moving to the region close to $X = 1$. Whilst this is observed to occur in the ensemble distributions for decreased values of F, after 30 years the parameter values remain unchanged; the change observed in the single trajectory is presumably influenced by the inclusion of points in years 30 to 45 of the model integration. The distribution in panel (m) shows a non-negligible probability (0.6%) of a trajectory occurring at a value $X < -0.5$; a region which has previously not been visited. The corresponding single trajectory distribution in panel (n) does not have any density in this region and therefore using a single model trajectory, with a limited number of data points, to estimate the entire PDF and associated exceedance probabilities is potentially misleading.

The mid-winter comparison demonstrates additional pitfalls in using a single model realisation, as opposed to an IC ensemble distribution, to understand the climate of the L84 model. The (c) and (g) panels in the third column show the ensemble distributions for X after 15 and 30 years respectively when there is no trend in the seasonal cycle of F. Whilst the corresponding single trajectory distributions in panels (d) and (h) are fairly similar and do not change markedly, neither of the distributions resemble the ensemble distributions sufficiently to justify using a single model trajectory to provide reliable quantitative probabilistic information. After 60 and 75 years, the single trajectory distributions in panels (p) and (t) show density in the region close to $X = 0$ whilst in the ensemble distributions in panels (o) and (s) there is very little density below $X = 0.5$. Again, this is likely due to the inclusion of earlier years in the single trajectory distributions but could equally be due to a limited sample size. Being unable to distinguish without further analysis is an unhelpful feature of using single trajectory distributions to investigate the model climate.

The changes in the statistics of the climate distributions over time, which map the evolving geometry of the pseudo-attractor, are not smooth. The irregular nature of the distributions means that comparing the single trajectory approach to the IC ensemble approach using traditional statistical measures such as means and variances can produce misleading information. The KS test is employed once again and the corresponding ensemble and single trajectory distributions in figure 4.27 are compared over the 75 year period. The results for mid-summer and mid-winter are given in figures 4.28(a) and 4.28(b) respectively. In general, the values of D are greater in the mid-winter comparisons than in the mid-summer comparisons. The values range from just below $D = 0.1$ to just below $D = 0.3$. This range is similar to that observed for the sample size of 30 points shown in figure 4.22 where the model evolves in the absence of a trend in F. It is not possible to conclude that the ergodic assumption becomes weaker in a climate change scenario based on these results alone. However, it is reasonable to conclude that a 30 year sample is insufficient to provide credible probabilistic information about the pseudo-attractor climate distributions.

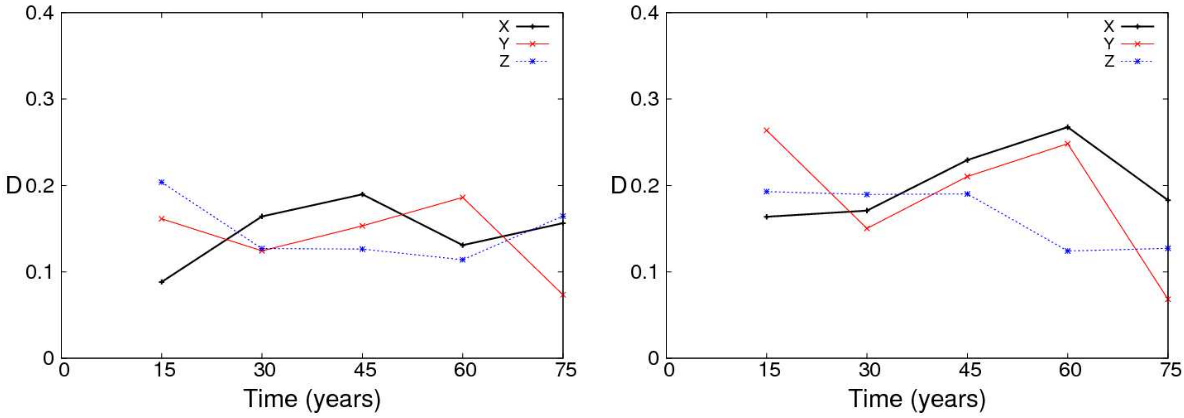

(a) Mid-summer

(b) Mid-winter

Figure 4.28: KS comparison between single trajectory distributions and respective IC ensemble distributions for the seasonally driven L84 model when subject to a trend in F (as shown in figure 4.25).

A major limitation of using a single model trajectory and invoking the ergodic assumption is that in creating a climatology, the data points used can span two or more very different underlying climates; effectively sampling different pseudo-attractors. Therefore the estimated probability distributions risk being misleading, even in the PMS. The implications of this for climate change impacts assessments are potentially important and are further discussed in section 4.6.

4.5.2 Influence of intransitivity on the L84 model under climate change

It is shown in section 4.4.3 that in the absence of a trend in the model's forcing, a 30 year sample is unlikely to be a long enough period to sample the irregular climate distributions associated with the seasonally driven L84 model. Furthermore, when a trend in the parameter F is introduced, section 4.5.1 demonstrates that relying on the statistics of a single model trajectory distribution is unsatisfactory as the changes in the geometry of the pseudo-attractor are not smooth, even with a linear trend in F. Additional experimental results with the L84 model reveal another reason why it is necessary to consider an ensemble of initial states, as opposed to a single model trajectory, when assessing the impact of climate change on the dynamic behaviour of the L84 model.

As the variation in F shifts towards lower values, model trajectories become exposed to qualitatively different regions of parameter space that are associated with intransitive behaviour (for fixed values of F). In an extension of the experiment outlined in section 4.5.1, the value of F is subject to a linear decreasing trend between 30 and 75 years but is then held constant at $F_m = 6$ for the following 75 years. The associated time series in F is illustrated in figure 4.29.

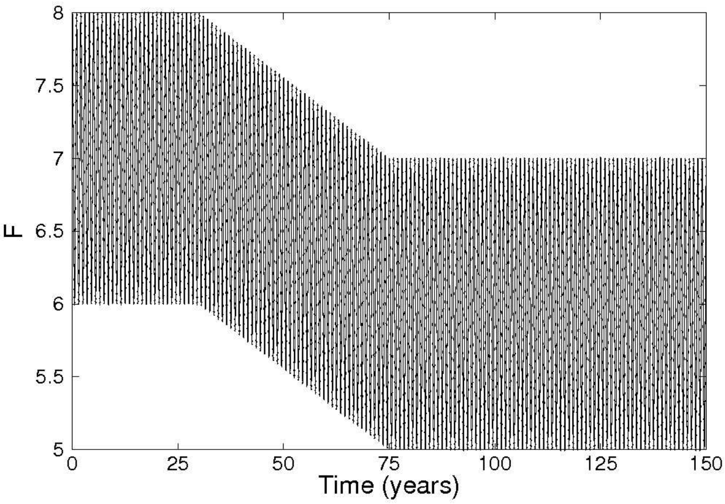

Figure 4.29: Time series in F over a 150 year period with a linear decrease between 30 and 75 years ($H = -0.0\dot{2}$) from $F_m = 7$ to $F_m = 6$.

When the IC ensemble illustrated in figure 4.26 evolves according to the changing parameter F shown in figure 4.29, after 75 years the vast majority of the IC members display constrained periodic oscillations associated with a pseudo-attractor (hereafter PA1, illustrated in figure 4.31) at the altered parameter setting, where $F_m = 6$ (with $M = 1$). However, there are a number of IC members that appear to be outliers in the decades after the trend in F has ceased. Figure 4.30 shows the evolution of three individual model trajectories over the 150 year simulation period. The time series in figure 4.30(a) shows the trajectory associated with the first member of the 10,000 member IC ensemble which displays behaviour that is typical of the majority of ensemble members. Initially, the trajectory demonstrates intermittency transitioning between periodic and aperiodic cycles spanning the range $-0.6 < X < 2.4$. This behaviour continues for the first 65 years of the model integration. During the latter part of the time series, when F_m is held constant, the trajectory displays dampened periodic oscillatory behaviour propagating in the range $0.5 < X < 1.5$ with the highest density of values in the range $0.9 < X < 1.2$. The time series' shown in figures 4.30(b) and 4.30(c) illustrate alternative model responses that are observed. At approximately 70 years into the model integration, as the trend in F approaches the new value of F_m, the two trajectories appear to develop according to a different, seemingly coexistent pseudo-attractor (hereafter PA2). The range of values is predominantly confined to the region $-0.3 < X < 1.9$ with occasional departures that extend to values close to $X = -0.5$ and $X = 2.5$. The results suggest that the model has two coexisting pseudo-attractors when

$F_m = 6$ and the model trajectories exhibit long-term memory of the initial state dictating the pseudo-attractor to which each trajectory evolves. PA1 appears to be a stable pseudo-attractor of the seasonally driven L84 model for $F_m = 6$ whilst PA2 is an unstable pseudo-attractor as all trajectories are observed to transition to PA1 over time (quantitative analysis presented in section 4.5.3).

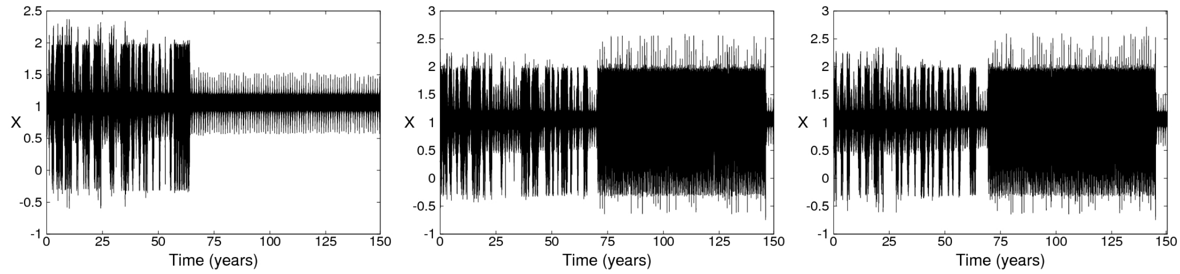

(a) IC member 1 (b) IC member 1099 (c) IC member 2054

Figure 4.30: Single trajectory results for the seasonally driven L84 model when subject to a parameter change given in figure 4.29, for given members of the IC ensemble.

The geometric properties of PA1, associated with the seasonally driven L84 model in the new climate regime where $F_m = 6$, are illustrated in figure 4.31. A single model realisation is run for one year starting from an IC on PA1. The resulting trajectory is shown in the X-Y, X-Z and Y-Z planes. The trajectory consists of a collection of ellipses which are reasonably well constrained in the X dimension and lie approximately parallel to the Y-Z plane. The plots are very similar to those shown for permanent summer conditions in figure 4.5 implying that PA1 consists of solutions which are modulations of the ellipse-like attractor, $A2$, observed when F is held constant at $F = 6$.

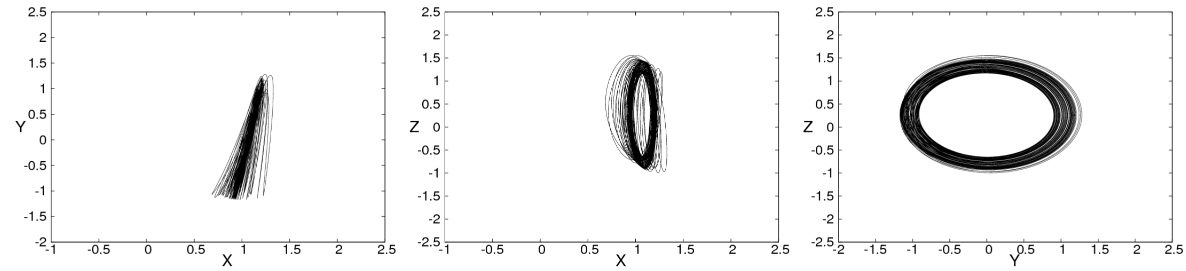

(a) X-Y Plane (b) X-Z Plane (c) Y-Z Plane

Figure 4.31: Pseudo-attractor, PA1, for the seasonally driven L84 model (with $M = 1$ and $F_m = 6$) for the X-Y, X-Z and Y-Z planes. The trajectory is run for one year beginning on January 1st with ICs $(0.90, -0.75, -1.19)$.

4.5.3 Memory of IC location

In this section the time scale at which trajectories evolving on PA2 transition to PA1 is investigated. A large IC ensemble is run for a 500 year simulation period under permanent summer conditions. The IC ensemble consists of 10,000 members spread evenly along a transect in the model state space, from $(-1.0, -2.5, -2.5)$ to $(2.5, 2.5, 2.5)$. The frequency distributions at the end of the 500 year simulation are given in figure 4.32 for each of the model variables in mid-summer and mid-winter. The range of X values in mid-summer and mid-winter is $0.64 < X < 1.35$ and $0.90 < X < 1.21$ respectively. The ranges of model states are therefore consistent with the ranges displayed in figure 4.31 suggesting that after a period of 500 years all 10,000 trajectories have transitioned towards PA1, which is intransitive and non-chaotic.

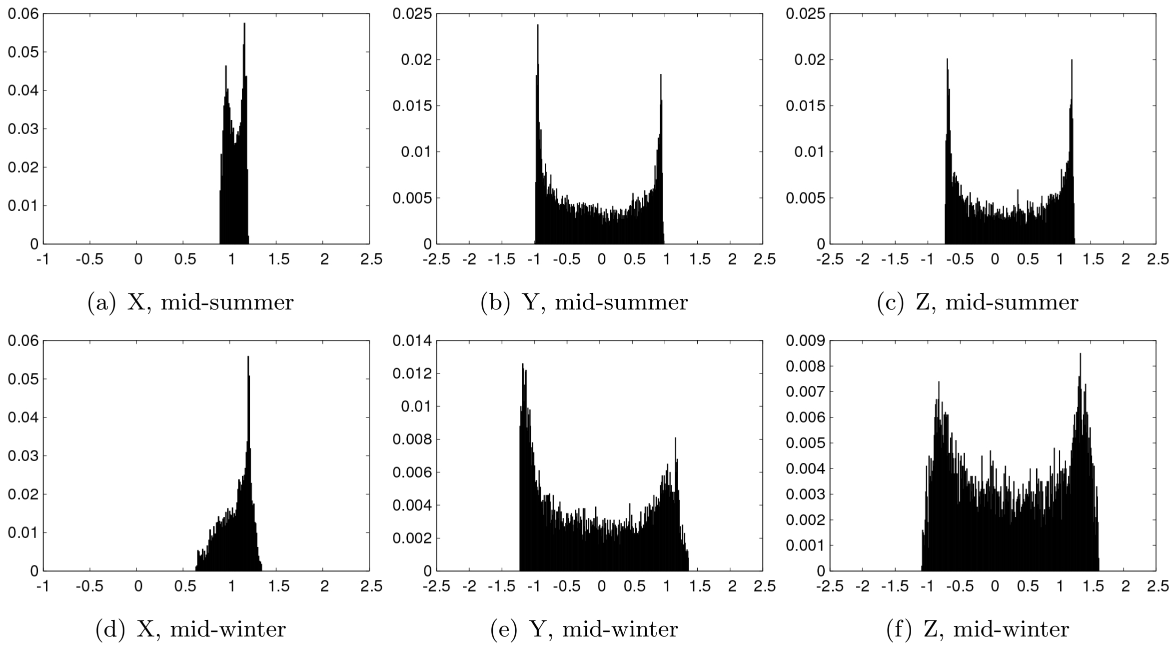

(a) X, mid-summer (b) Y, mid-summer (c) Z, mid-summer

(d) X, mid-winter (e) Y, mid-winter (f) Z, mid-winter

Figure 4.32: Normalised frequency distributions of a 10,000 member IC ensemble for the seasonally driven L84 model in mid-summer, (a) to (c), and mid-winter, (d) to (f), after a 500 year simulation with $M = 1$ and $F_m = 6$. In each plot, the x-axis denotes the X variable and the y-axis corresponds to the frequency per occupied bin; bin width = 0.01.

An extension of the experiment outlined in section 4.5.2 is performed to determine the rate at which the IC ensemble converges towards the distribution of model states consistent with PA1. When subject to the trend in F implemented in section 4.5.2, the percentage of trajectories originating from the IC ensemble (shown in figure 4.26) that fall outside the identified ranges in X for mid-summer and mid-winter consistent with PA1 (as shown in figure 4.32) are determined over the period from 75 years to 125 years. After the instant at 75 years in which the trend in F stops, if a trajectory from the ensemble lies outside the identified ranges for the X, it is assumed that the trajectory is evolving on PA2. Of course, at any given time a trajectory evolving on PA2 may pass through the range associated with PA1 so the estimated percentage of trajectories on PA2 is an underestimate. However, the rate at which trajectories converge to PA1 can still be estimated given the rate of change in the relative number of trajectories inside and outside the ranges.

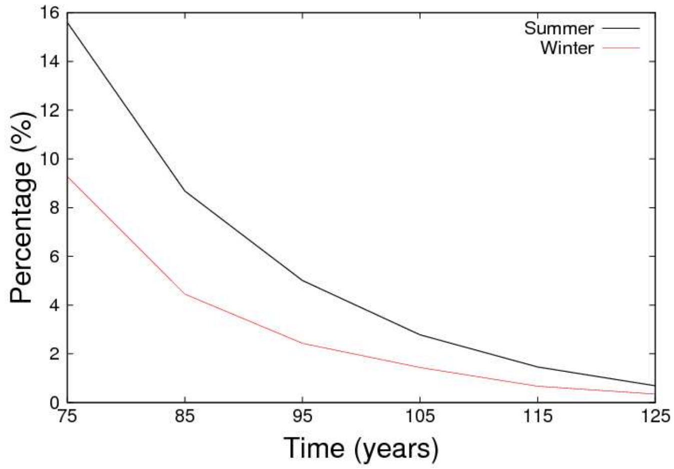

Figure 4.33: Percentage of trajectories from the IC ensemble shown in figure 4.26 not yet evolving on PA1 following the stabilisation of F at $F_m = 6$, consistent with the trend in figure 4.29.

Figure 4.33 shows the combined percentage of trajectories above and below the specified ranges in X identified for PA1 over a 50 year period following stabilisation of the trend in F at $F_m = 6$. Typically more ensemble members are found below the minimum values of $X = 0.9$ in mid-summer and $X = 0.64$ in mid-winter than above the upper thresholds of $X = 1.21$ and $X = 1.35$ respectively. The percentages are systematically greater during mid-summer, largely because the range of values associated with PA1 during mid-summer is smaller than the range associated with PA1 during mid-winter. The plots show exponential-like decreases in the percentage of ensemble members continuing to evolve on PA2. However, even 50 years after the altered parameter configuration has become established, not all trajectories have transitioned to PA1 suggesting multi-decadal memory in the L84 model under altered parameter conditions.

In the analogy to modelling of the climate system, it is pertinent to ask what relevance such results have for predicting climate change. In addition to the arguments previously set out for invalidating the ergodic assumption, the results suggest that the behaviour of single model trajectories from different initial states can differ considerably when the system is forced into a region of parameter space containing coexisting stable (and unstable) pseudo-attractors. The frequency distributions associated with the single trajectories can therefore only sample a subset of the possible climate states consistent with the forcing under a particular climate change forcing scenario. In the seasonally driven L84 model under transient parameter changes, the emergence of alternative model trajectory responses only became evident when running large IC ensembles. It is therefore important to account for the potential long-term memory of the initial state of the system when predicting climate change by implementing large IC ensemble experiments.

4.6 Implications for Climate Prediction

In analysing the experiments conducted with the L84 model, it is immediately apparent that despite the model's low dimensionality, the model displays enormously rich and interesting dynamic behaviour. The analysis presented in this chapter suggests that understanding and ultimately predicting the evolution of a nonlinear system's climate becomes more challenging when dealing with time-varying parameters. The following discussion relates the issues identified using the L84 model to the predictability of the climate system under climate change. The discussion focusses on three themes which are addressed in this chapter; the coexistence of attractors, the ergodic assumption and the long-term memory of the initial state.

4.6.1 Coexisting attractors

The coexistence of attractors presents significant problems for prediction in nonlinear dynamic systems. If the climate system has coexisting attractors then it is pertinent to ask whether or not IC uncertainty, which has previously been considered relatively unimportant for long-term climate prediction (Cox and Stephenson (2007), Hawkins and Sutton (2009)), impedes the accurate prediction of future climate states using existing climate model experimental designs. Whilst a definitive answer regarding the potential of the climate system to have two or more coexisting attractors is currently elusive, scientists have inferred the possibility of coexisting climate regimes using insights from palaeoclimatology. Over four decades ago, Budyko (1969) stated:

> "With the present distribution of continents and oceans the existence of two climatic regimes is possible: one of which is characterised by the presence of polar ice and large thermal contrast between the pole and equator, and the other by the absence of glaciation and small meridional mean gradient of temperature."

To link the possibility of the coexisting regimes identified by Budyko (1969) to the coexistence of climate attractors is speculative. However in considering the potential for the climate system to exhibit multistability on a number of spatial and temporal scales, the notion of coexisting attractors is a relevant and useful concept. The experiments with the L84 model have highlighted some of the nuanced behaviour that can exist in a system displaying both transitive and intransitive behaviour associated with a single attractor and multiple coexisting attractors respectively.

In section 4.2.3, two coexisting attractors are illustrated for permanent summer parameter forcings and figure 4.6 shows the complicated structure of the basins of attraction. Given uncertainty in the initial model state, the results show that estimating the probability of a trajectory propagating to one of the two attractors, requires a detailed exploration of the model state space.

Recently, Freire et al. (2008) used bifurcation analysis to report phase diagrams of the L84 model which reveal highly complex behaviour and unlike the basins of attraction shown in figure 4.6, the Freire et al. (2008) study shows regions of parameter space where the basins of attraction contain up to *four* coexisting attractors. The authors conclude that the precise tuning of parameters is paramount in establishing the number of coexisting attractors in the L84 model. In addition, both Lorenz (1990) and Freire et al. (2008) suggest that the basins of attraction are complicated with the latter study referring to "foliated" structures, suggesting the presence of the Wada property. Whilst the L84 model does not strictly possess the Wada property in permanent summer conditions (when $F = 6$), the basins of attraction have a complicated structure inevitably influencing the convergence of IC ensemble distributions and single trajectory distributions. The Wada property is similar to an even more daunting concept for climate modellers, "riddled basins", which refer to basins of attraction which are "so densely intertwined that it may be virtually impossible to determine the final state" (Viana et al. (2009)). The combination of coexisting attractors, the number of which can be highly sensitive to parameter choice, and the prospect of riddled basins, or the Wada property, which ensures that the attractor to which a trajectory evolves is sensitively dependent on the initial state, presents a problematic situation for the climate modelling community.

Pseudo-attractors

In section 4.4, the L84 model is subject to smooth variations in the forcing parameter F. The consequence is to impose regular transitions between chaotic and non-chaotic regions of parameter space. The seasonal cycle investigated ($6 < F < 8$), effectively created a "pseudo-attractor" which is ultimately transitive, as all points in the pseudo-attractor state space are visited over a long integration period (see section 4.4.2). The ensemble distributions for mid-summer and mid-winter, with a seasonal cycle in F, are shown to be different to the permanent summer and permanent winter ensemble distributions. In the climate system, we may expect chaos to be a permanent feature of the atmospheric circulation throughout the year but the impact of a continuously changing forcing may well alter the geometric properties of any climate attractor. Therefore the concept of a pseudo-attractor may be more apt in the analogy to climate change; a significant change in the geometry of the system's pseudo-attractor would indicate a change in climate.

An extension of the possibility for coexisting attractors would be the coexistence of pseudo-attractors. It is observed that multiple pseudo-attractors coexist (albeit temporarily) following the transient phase of the experiment in section 4.5.1. Once the final parameter conditions are established, and the F parameter oscillated between $5 < F < 7$, there is evidence of two coexisting pseudo-attractors (PA1 and PA2), which initially appeared intransitive over the following decades for certain ensemble members. The observation of long-term memory in the forced L84 model stresses the importance of adequately representing IC uncertainty to generate robust distributions for model variables under altered forcings. Further discussion of the memory in the L84 model is given in section 4.6.3.

4.6.2 The ergodic assumption: lessons from L84

For a chaotic transitive system the ergodic assumption is valid, as shown in the L63 model with conventional fixed parameter values and demonstrated in section 4.3.2 for the L84 model evolving under permanent winter parameter conditions. The convergence of the single trajectory distributions to the IC ensemble distributions is fairly rapid and only requires a simulation period of a few months (see section 4.3.3). In permanent summer conditions however, the ergodic assumption is inappropriate. As the system is non-chaotic and two periodic attractors coexist, the intransitive behaviour of the model means that the ensemble distributions incorporate regions of state space that are not observed for individual single trajectories.

Further experiments with the L84 model demonstrated that ergodicity is not observed when using data that is inconsistent with the underlying parameter conditions. In section 4.4.3, the seasonally driven L84 model is investigated and the time scale at which the frequency distributions of a single model trajectory converged to the IC ensemble distributions is estimated to be on the order of a few hundred years under fixed parameter conditions (with one data point used per year). Distributions from shorter simulation periods do not converge to the ensemble distributions. In an attempt to speed up the convergence time, additional data from all time steps in January and July are included in the single trajectory distributions for winter and summer respectively. The distributions, given in section 4.4.4, do not fully converge to the IC ensemble distributions centred on mid-winter and mid-summer. The reason for the discrepancies is that the single trajectory distributions include data points which are never observed at mid-winter and mid-summer. Incorporating data from time instants in which the parameter fluctuations differ to those at the time of interest risks producing misleading PDFs of the model climate.

The active use of the ergodic assumption, as an alternative to running large IC ensembles, may be founded in a belief that climate variability, at a particular scale of interest, is insensitive to the forcing scenario and any change in the distribution of a particular variable is likely to be smooth in time. In section 4.5.1, a linear trend in F is imposed on the seasonal cycle in F. The IC ensemble distributions illustrated in figure 4.27 change dramatically over the 45 years in which the trend is present. Whilst the single trajectory distributions also change over the period, the changes are not always consistent with the ensemble distributions. This is partly caused by a limited sample of data points but is also a consequence of including data from instances when the model trajectory is evolving towards different attractors. The former point is simply a statistical problem pervasive across all domains of science but the latter point has specific significance to climate modelling. If the attractor (or pseudo-attractor) associated with the climate system changes in an irregular fashion, then any PDF that is derived from a time-averaged distribution of a single model trajectory will be fundamentally flawed. The resulting probabilities will therefore be misleading and estimates of threshold exceedance will be incorrect; an important consideration for the adaptation user community (particularly insurers) when utilising climate model output.

As described in section 4.5.1, the ergodic assumption is invalid when simulating a change in climate from transitive to intransitive model behaviour. If the future climate scenario consists of a pseudo-attractor that is transitive and varies smoothly in response to a trend in a climate forcing, then the ergodic hypothesis would not necessarily fail. The ergodic assumption would remain valid for a time series in which variability about some mean value is stationary over time but in the context of a changing climate, particularly at regional scales where changes are often nonlinear and abrupt, the stationarity of climate variability under climate change is unlikely. In relating the concepts explored in this chapter to climate prediction, an important question that arises is whether or not we expect the distribution of climate (inexorably linked to climate variability) to vary smoothly and predictability over time in response to an external forcing. If not, then the results in this chapter suggest that climate model experiments must take account of IC uncertainty to explore the changing geometry of climate distributions consistent with the climate's pseudo-attractor(s).

4.6.3 Memory of ICs

There is inevitable uncertainty in the observable initial state of the atmosphere-ocean system. In developing climate change adaptation strategies, it is advantageous to know the full range of possible future states of the climate. Therefore, even if different model trajectory ICs evolve towards different attractors consistent with a future forcing scenario, it is important to know the range of plausible future states conditioned on the current uncertainty in the initial state. In examining the sensitivity of the climate to the uncertainty in the initial state, the notion of system memory therefore becomes a relevant consideration. In seeking predictive skill, knowing the time scale over which uncertainty in the initial state is lost can provide climate modellers with a time horizon for the extent of successful climate prediction, over and above considering all states which are plausible given certain forcing scenarios.

By initially considering intransitive behaviour with the L84 model in parameter regions not exposed to chaos, it was demonstrated that knowledge of the initial state is crucial in estimating the model climate. If the climate system, or sub-systems of the climate system, are exposed to the possibility of intransitive coexisting (pseudo-)attractors, then single model realisations will only ever sample one (pseudo-)attractor. In section 4.3.3, it is shown that during permanent summer conditions, the convergence of ensembles is affected by memory of the ICs. The future distribution of states associated with a single model trajectory is entirely determined by the initial state of the model. An IC ensemble approach to predicting the model's climate would therefore generate distributions that span more than one coexisting climate, provided the ICs cross the boundaries of the basins of attraction. Therefore, if there is uncertainty in the initial state, there is a danger in relying on the variability of a single model realisation to inform on the range of future possible model states.

In creating an analogy to climate change, the analysis presented in section 4.5 focusses on the impact of a linear trend in F that moves the model into a more summer-like configuration. As referred to in section 4.6.1, in the new climate where $F_m = 6$ the model shows memory of the ICs which extended over many decades. Over time all trajectories evolve towards PA1 but temporarily some trajectories evolve on PA2. The existence of long-term memory exhibited by certain trajectories in the L84 model suggests that in transitioning to a new climate, trajectories can become trapped in an apparently anomalous pattern. In estimating the probabilities associated with the model, it would therefore be misleading to consider only one (or a few) model realisations. Clearly, unanticipated behaviour can result when model parameters or system forcings vary in time. In modelling the climate system, using IC ensembles might help to elicit possible dynamic behaviour that results from different ICs and guide the suitable extraction of quantitative probabilistic information from climate model output.

The parameter space explored in section 4.5 is subject to intransitive, non-chaotic behaviour. It is therefore sensible to determine what relevance such an exercise can have for the real climate system which is known to display chaotic behaviour. As an example, one could consider the potential for regional climates to display intransitivity. Certain feedbacks in the climate system have the potential to lead to intransitive behaviour and one could argue that certain feedbacks are highly sensitive to the initial state of the atmosphere-ocean system. For example, in certain regions of the world which are highly sensitive to the hydrological cycle, rainforest conditions are potentially coexistent with savannah conditions. An example where much research has recently been focussed is the destabilisation of regions of the Amazon rainforest in response to future climate change and deforestation (Betts et al. (2008)). Therefore when projecting the impacts of climate change as a response to altered forcings, it is not irrelevant to consider the potential consequences of intransitive behaviour. A related concept which is explored in the following chapter is almost-intransitivity; a feature of a dynamical system which is ultimately transitive but displays long-term IC-dependent behaviour. The relation of almost-intransitivity to memory and climate predictability is considered in the analysis presented in chapter 5 using the L84 model coupled to the Stommel ocean box model (Van Veen et al. (2001)).

4.6.4 Conclusions from the L84 experiments

So what do the results of the L84 experiments reveal about the predictability of the climate system and what lessons are there for the climate modelling and adaptation communities? Ultimately, the L84 model results suggest that no climate change modelling exercise is complete without fully taking into account uncertain ICs. The experiments conducted with L84 model suggest that ignoring the impact of nonlinearities in the climate system, and their interaction with time-varying parameters, could lead to a distorted view of climate change. The concept of a pseudo-attractor can help to conceptualise the dynamic behaviour of a time-dependent system undergoing change in response to changes in external forcings.

The results in the L84 model have focussed on the PMS. In the IMS, ensemble methods sometimes account for uncertainty by perturbing parameters. However, an ensemble modelling approach based on sampling parameter uncertainty without accounting for IC uncertainty, and relying on the data from single model realisations, risks providing misleading information which doesn't take into account the potential memory of the initial model state. Results with the L84 model suggest that without fully assessing the consequences of uncertainty in the initial state, it is difficult to generate relevant quantitative information about the future state of the climate system for decision makers.